Development 140, 3285-3296 (2013) doi:10.1242/dev.090266

Three-dimensional culture and cAMP signaling promote the maturation of human pluripotent stem cell-derived hepatocytes

Shinichiro Ogawa[1], James Surapisitchat[1], Carl Virtanen[2], Mina Ogawa[1], Maryam Niapour[1], Kim S. Sugamori[3], Shuang Wang[3], Laura Tamblyn[3], Chantal Guillemette[4], Ewa Hoffmann[3], Bin Zhao[3], Stephen Strom[5], Rebecca R. Laposa[3], Rachel F. Tyndale[3], Denis M. Grant[3] and Gordon Keller[1,*]

SUMMARY

Human pluripotent stem cells (hPSCs) represent a novel source of hepatocytes for drug metabolism studies and cell-based therapy for the treatment of liver diseases. These applications are, however, dependent on the ability to generate mature metabolically functional cells from the hPSCs. Reproducible and efficient generation of such cells has been challenging to date, owing to the fact that the regulatory pathways that control hepatocyte maturation are poorly understood. Here, we show that the combination of three-dimensional cell aggregation and cAMP signaling enhance the maturation of hPSC-derived hepatoblasts to a hepatocyte-like population that displays expression profiles and metabolic enzyme levels comparable to those of primary human hepatocytes. Importantly, we also demonstrate that generation of the hepatoblast population capable of responding to cAMP is dependent on appropriate activin/nodal signaling in the definitive endoderm at early stages of differentiation. Together, these findings provide new insights into the pathways that regulate maturation of hPSC-derived hepatocytes and in doing so provide a simple and reproducible approach for generating metabolically functional cell populations.

KEY WORDS: Endoderm, Hepatocyte, Human pluripotent stem cell, Maturation, Three dimensional culture, cAMP signaling

INTRODUCTION

The ability to direct the differentiation of human pluripotent stem cells (hPSCs) (embryonic and induced pluripotent stem cells) to specific lineages in culture does provide access to unlimited numbers of human primary cells for a wide range of applications that include the development of new treatments for a spectrum of diseases, the establishment of platforms for drug discovery and predictive toxicology, and the creation of *in vitro* models of human disease. Among the different lineages that can be derived from hPSCs, hepatocytes are of particular importance as they are the cells responsible for drug metabolism and thus for controlling xenobiotic elimination from the body (Guillouzo, 1998; Gebhardt et al., 2003; Hewitt et al., 2007). Given this role and the fact that individuals can differ in drug-metabolizing capacity (Byers et al., 2007), access to functional hepatocytes from a representative population sample would greatly facilitate drug discovery and testing within the pharmaceutical industry. Additionally, hepatocyte transplantation and bio-artificial liver devices developed with hPSC-derived hepatocytes represent potential life-saving therapies for individuals with specific types of liver disease who have no available matched donor organ.

[1]McEwen Centre For Regenerative Medicine, University Health Network, Toronto, ON M5G 1L7, Canada. [2]Toronto General Hospital Research Institute, University Health Network Microarray Center, University Health Network, Toronto, ON M5S 1A8, Canada. [3]Department of Pharmacology and Toxicology, Faculty of Medicine, University of Toronto, Toronto, ON M5S 1A8, Canada. [4]Faculty of Pharmacy, Laval University, CHUQ Research Center, 2705, Boulevard Laurier, Room T3-48, Quebec, QC G1V 4G2, Canada. [5]Karolinska Institutet, Department of Laboratory Medicine, Division of Pathology, F56, Karolinska, University Hospital, Stockholm SE-141 86, Sweden.

*Author for correspondence (gkeller@uhnresearch.ca)

Accepted 24 May 2013

Given the potential therapeutic and commercial importance of functional human hepatocytes, significant effort has been directed towards optimizing protocols for the generation of these cells from hPSCs over the past five years (Cai et al., 2007; Duan et al., 2007; Hay et al., 2008; Basma et al., 2009; Duan et al., 2010; Si-Tayeb et al., 2010b; Sullivan et al., 2010; Touboul et al., 2010; Chen et al., 2012). Almost all approaches have attempted to recapitulate the key stages of liver development in the differentiation cultures, including the induction of definitive endoderm, the specification of the endoderm to a hepatic fate, the generation of hepatic progenitors known as hepatoblasts and the differentiation of hepatoblasts to mature hepatocytes (Si-Tayeb et al., 2010a). In most studies, differentiation is induced in a monolayer format with the sequential addition of pathway agonists and antagonists that are known to regulate the early stages of development, including endoderm induction and hepatic specification. In contrast to the early developmental steps, the signaling pathways that promote the maturation of the hPSC-derived hepatocytes to functional cells as defined by Phase I and Phase II drug-metabolizing enzyme activity have not been well defined. As a consequence, the populations produced with the different protocols vary considerably in their maturation status and in most cases represent immature hepatocytes. The inability to reproducibly generate mature cells represents a significant bottleneck in the field, as drug development applications require cells that display functional levels of key drug-metabolizing enzymes.

In this study, we have addressed the issue of maturation by manipulating specific signaling pathways at different stages of hepatic development in hPSC differentiation cultures. We show that sustained activin/nodal signaling is important for appropriate patterning of the definitive endoderm population for hepatic specification, and that three-dimensional (3D) cellular aggregation of hepatoblast-stage cells initiates maturation of this progenitor

population. Finally, we demonstrate that cAMP signaling within the 3D hepatoblast aggregates promotes further maturation to functional stage cells, as demonstrated by the upregulation of selected drug-metabolizing enzymes, including several Phase I cytochrome P450 and the Phase II enzymes that are responsible for the metabolism of many clinically and toxicologically important drugs.

MATERIALS AND METHODS

Human PSC culture and differentiation

hPSCs were maintained on irradiated mouse embryonic feeder cells in hESC medium as described previously (Kennedy et al., 2007). Prior to the generation of embryoid bodies (EBs), hESCs were passaged onto Matrigel-coated plates for 1 day to deplete the population of feeder cells and then dissociated with 0.25% Trypsin-EDTA to generate small clusters as previously described (Kennedy et al., 2007; Nostro et al., 2011). The clusters were cultured in serum-free differentiation (SFD) medium in the presence of BMP4 (3 ng/ml) for 24 hours (day 0 to day 1) and then in differentiation medium consisting of StemPro-34 supplemented with glutamine (2 mM), ascorbic acid (50 μg/ml; Sigma), MTG (4.5×10^{-4} M; Sigma), basic fibroblast growth factor (bFGF; 2.5 ng/ml), activin A (100 ng/ml), Wnt3a (25 ng/ml) and BMP4 (0.25 ng/ml) for 3 days. On day 4, the medium was changed and the amount of bFGF was increased to 5 ng/ml for an additional 48 hours of culture. At this stage, the EBs were harvested and dissociated with 0.25% Trypsin-EDTA and the cells cultured for 2 days on Matrigel-coated 12-well plates at a concentration of 4×10^5 cells in above differentiation medium without Wnt3A and a reduced amount of activin (50 ng/ml). On day 8, the differentiation medium was replaced with hepatic specification medium that consisted of Iscove's Modified Dulbecco's Medium (IMDM) supplement with 1% vol/vol B27 supplement (Invitrogen: A11576SA), ascorbic acid, MTG, FGF10 (50 ng/ml) (from day 8 to day 10), bFGF (20 ng/ml) (from day 10 to day 14) and BMP4 (50 ng/ml) (from day 8 to day 14). The medium was changed every 2 days until day 14 at which stage it was changed to maturation medium that consisted of IMDM with 1% vol/vol B27 supplement, ascorbic acid, glutamine, MTG, hepatocyte growth factor (HGF) (20 ng/ml), dexamethasone (Dex) (40 ng/ml) and oncostatin M (20 ng/ml). On day 26, the cells were dissociated with enzymatic treatment (collagenase type 1: Sigma C0130) and manual dissociation, and then cultured in six-well ultra-low cluster dishes at a concentration of 6×10^5 cells per well in above maturation medium supplemented with Rho-kinase inhibitor and 0.1% BSA to generate 3D aggregates. Aggregates were maintained under these conditions for 6 days, with medium changes every 3 days. On day 32, aggregates were cultured in hepatocyte culture medium (HCM) (Lonza: CC-4182) without EGF to promote the final stages of maturation. At this time point, 1 mM 8 bromo-cAMP (Biolog: B007) was added and the medium was changed every 3 days. To generate hepatocyte-like cells from H9 hESCs, H1 hESCs and 38-2 IPSCs, the following changes (summarized in supplementary material Table S1) were made to the hepatic specification medium. The concentration of bFGF was increased to 40 ng/ml and the base medium was switched from IMDM to H16 DMEM for culture from days 8-14 and then to H16 DMEM plus 25% Ham's F12 and 0.1% BSA from days 14-20. IMDM was replaced with H21 DMEM plus 25% Ham's F12 and 0.1% BSA for the maturation medium used from days 20-32. All cytokines were human and purchased from R&D Systems, unless stated otherwise. EB and monolayer cultures were maintained in a 5% CO_2/5% O_2/90% N_2 environment. Aggregation cultures were maintained in a 5% CO_2/ambient air environment.

Flow cytometry

Flow cytometric analyses were performed as described (Nostro et al., 2011). For cell surface markers, staining was carried out in PBS with 10% FCS, whereas for intracellular proteins, staining was performed on cells fixed with 4% paraformaldehyde (Electron Microscopy Science, Hatfield, PA, USA) in PBS. The conditions for SOX17 and FOXA2 staining were as previously described (Nostro et al., 2011). Albumin and α-fetoprotein staining was carried out in PBS with 10% FCS and 0.5% saponin (Sigma). Stained cells were analyzed using an LSRII flow cytometer (BD). The sources and concentrations of primary, secondary and isotype control antibodies are listed in supplementary material Table S7.

Immunostaining

To detect albumin and α-fetoprotein-positive cells, the populations were stained for 1 hour at room temperature with either a goat anti-ALB (Bethyl) or a rabbit anti-AFP antibody (DAKO). Concentrations of isotype controls were matched to primary antibodies. To visualize the signal, the cells were subsequently incubated for 1 hour at room temperature with either a donkey-anti-goat Alexa 488 (Invitrogen) or a donkey anti-rabbit-Cy3 antibody (Jackson ImmunoResearch). For SOX17 staining, the cells were fixed, permeabilized and blocked as described above. The stained cells were visualized using a fluorescence microscope (Leica CTR6000) and images captured using the Leica Application Suite software. For staining of the aggregates, they were fixed with 4% PFA at 37°C overnight, washed with normal saline (0.85% NaCl) and then embedded in 2% agar. The agar block was fixed with 10% PFA for 24 hours and embedded in a paraffin block and sectioned. For immunohistochemistry, the paraffin-embedded sections were dewaxed with xylene, rehydrated, placed in Tris-EGTA-buffer (TES; 10 mM Tris, 0.5 mM EGTA, pH 9.0) and subjected to heat-induced (microwave) epitope retrieval. The tissues were blocked by incubation with 10% normal donkey (Jackson ImmunoResearch) (for ALB/ASGR1, ALB/AFP and ALB/HNF4α staining) or goat serum (Jackson ImmunoResearch) (for ALB/E-cadherin staining) for 30 minutes. They were subsequently incubated with goat anti-ASGR1 (Santa Cruz), mouse-anti-E cadherin (BD) and goat anti-HNF4α (Santa Cruz) overnight at 4°C and then with anti-ALB and anti-AFP antibodies for 1 hour at room temperature. For double staining of ALB/ASGR1, ALB/AFP and ALB/HNF4α, the signals were visualized using donkey anti-goat Alexa 488 and anti-rabbit Cy3 antibodies. For ALB/E cadherin, the signals were visualized using goat anti-rabbit Alexa 488 and goat anti-mouse Cy3. The stained cells were analyzed using a confocal fluorescence microscope (Olympus Fluo View 1000 B laser scanning confocal) and images captured using the Olympus Application software. Primary and secondary antibodies were diluted in PBS+0.2% BSA+0.05% Triton-X100. Prolong Gold Antifade with DAPI (Invitrogen) was used to counterstain the nuclei.

Generation and dissociation procedure of 3D aggregates

Aggregates were generated from the monolayer by a combination of enzymatic treatment (collagenase type 1: Sigma C0130) and manual dissociation. For dissociation of the day 44 aggregates, they were incubated by gentle shaking overnight at room temperature in Hank's solution containing 1 mg/ ml collagenase Type II (Worthington #LS004176). On the following day, the solution was replaced with fresh dissociation medium consisting of Hank's solution supplemented with 10 mM taurine, 0.1 mM EGTA, 1 mg/ml BSA and 1 mg/ml collagenase type II. The cells were dissociated by gentle pipetting.

Quantitative real-time PCR

Total RNA was prepared using RNA aqueous Micro Kit (Ambion) and treated with RNase-free DNase (Ambion). RNA (500 ng to 1 μg) was reverse transcribed into cDNA using random hexamers and Oligo(dT) with Superscript III Reverse Transcriptase (Invitrogen). QPCR was performed on a MasterCycler EP RealPlex (Eppendorf) using a QuantiFast SYBR Green PCR Kit (Quiagen) as described previously (Nostro et al., 2011). Expression levels were normalized to the housekeeping gene TATA box-binding protein (*TBP*). For UGT1A1, expression was calculated using the delta-delta CT method relative to the level in non-treated (8-Br-cAMP) cells. Oligonucleotide sequences are available in supplementary material Table S8. For controls, two samples of total adult and fetal liver RNA were purchased from Clontech (AL1, FL1), Agilent Technologies (AL2) and BioChain (FL2). Two of the primary hepatocyte samples (HH1892 and HH1901) used for RNA analyses were generated by culture of freshly isolated hepatocytes, as previously described (Kostrubsky et al., 1999). A third sample was purchased from Zenbio (lot: 2199). All RNA information is available in supplementary material Table S8.

Indocyanine green uptake

The indocyanine green (ICG, Sigma) solution was dissolved in HCM (Lonza) at a concentration of 5 mg/ml and added to the cells at final concentration of 1 mg/ml ICG in HCM. The cells were incubated at 37°C for 1 hour, washed three times with PBS and then examined with an inverted

Microscope (Leica). To monitor release of the ICG, the cells were cultured in fresh medium without ICG for an additional for 24 hours.

Periodic acid-Schiff staining for glycogen

Cultured cells were fixed in 4% PFA for 15 minutes and stained according to the manufacturer's instructions using a Periodic acid-Schiff (PAS) staining kit (Sigma).

Albumin secretion assay

Medium was harvested following 24 hours of culture of the different cell populations and the amount of albumin secreted was measured according to the manufacturer's protocol using the Human Albumin ELISA Quantitation kit (Bethy Laboratories).

Drug metabolism assay by HPLC

Three lots of cryopreserved human hepatocytes (Celsis *In Vitro* Technologies, Baltimore, USA, lot No ONQ, OSI and JGM) were used as control. Cells were thawed and cultured in type 1 collagen-coated microtiter wells (5×10^4 cells per well) in InVitroGro HI medium (Celsis *In Vitro* Technologies) (Roymans et al., 2004). Following hepatocyte attachment (2-4 hours) the nonadherent dead cells were removed and replaced with fresh medium. To measure CYP1A2 and CYP3A4 induction, the primary hepatocytes (lots OSI and JGM) or hPSC-derived aggregates were treated with either lansoprazole (10 μM) or rifampicin (10 μM) for 72 hours. Medium with fresh inducer was changed daily. Following induction, the cells were incubated in the medium containing either the CYP1A2 substrate phenacetin (200 μM) or the CYP3A4 substrate testosterone (250 μM) for 24 or 2 hours, respectively. After incubation, aliquots of the medium were collected and the levels of metabolites were quantified by high-performance liquid chromatography. Controls were cultured with DMSO alone (final concentration 0.1%). Following the metabolic assays, the aggregates were harvested, dissociated and the cells counted.

To measure the CYP2B6, NAT1/2 and Total UGT activities, the hPSC-derived aggregates and cryopreserved hepatocytes (lot ONQ) were incubated in medium containing either the CYP2B6 substrate bupropion (900 μM), the NAT2- selective substrate sulfamethazine (SMZ) (500 μM) or the total UGT substrate 4- methylumbeliferone (4-MU) (200 μM) for either 24 or 48 hours. Hydroxybupropion, *N*-acetyl-SMZ and 4-MU glucuronide levels were quantified by HPLC using the methods of Loboz et al. (Loboz et al., 2005), Grant et al. (Grant et al., 1991) and Gagné et al. (Gagné et al., 2002), respectively.

Microarray processing and data analysis

RNA samples were run on Affymetrix Human Gene ST v1.0 chips following standard Affymetrix guidelines at the University Health Network Genomics Centre. Briefly, 300 ng of total RNA starting material for each sample was used as input to the Ambion WT Expression Kit. Amplified cDNA (2.7 μg) was then fragmented, labeled and hydridized to Affymetrix Human Gene ST v1.0 chips for 18 hours (45°C at 60 rpm). Arrays were washed using a GeneChip Fluidics Station and scanned with an Affymetrix GeneChip Scanner 7G. Raw CEL files were imported into Genespring (Agilent, v11.5.1) and probe level data were summarized using the ExonRMA16 algorithm based on the HuGene-1_0-st0v1_na31_hg19_2010-09-03 build. Each gene was normalized to the median value across all samples under consideration. All statistics were performed on log 2 transformed data. In total, 28,869 transcripts are represented on this array.

As a first step, transcripts were filtered to remove those that were consistently in the lower 20th percentile of measured expression across all of the three sample groups. An unsupervised hierarchical clustering analysis with a Pearson centered distance metric under average linkage rules was used to address overall similarity and differences between the samples and groups. Directed statistical analysis between the three sample groups was performed by ANOVA with a Benjamini and Hochberg False Discovery Rate (FDR, $q<0.05$) (Klipper-Aurbach et al., 1995). To find sets of differentially expressed transcripts with biological meaning, a gene ontology (GO) analysis was performed using a corrected Benjamini and Yuketieli hypergeometric test at the $q<0.1$ significance level (Benjamini et al., 2001). Two *a priori* defined sets of specific transcripts were examined in more detail: transcripts related to specific liver-related activity of interest; and transcripts found to be expressed and liver specific based on publicly available information from the HOMER database (Zhang and Chen, 2011). Microarray data have been deposited in GEO with Accession Number GSE39157.

RESULTS

Endoderm induction in EBs

The protocol to generate functional hepatocyte-like cells was developed with the HES2 hESC line using the embryoid body (EB) format for the early induction steps (Fig. 1A). Using this approach, EBs generated in the presence of BMP4 (24 hours) are exposed to activin A (activin) and Wnt3a for 5 days to induce definitive endoderm, a population defined by expression of the surface markers CXCR4, CKIT and EPCAM and the transcription factors SOX17 and FOXA2. Under optimal conditions, $CKIT^+CXCR4^+$, $SOX17^+$ and $FOXA2^+$ cells were detected within the EBs by day 3 of differentiation, and their number increased dramatically over the next 72 hours (Fig. 1B). By day 6 of differentiation, over 95% of the induced EB population co-expressed CXCR4 and CKIT or CXCR4 and EPCAM (Fig. 1B; supplementary material Fig. S1A). Intracellular flow cytometric analyses revealed that more than 95% of the cells expressed SOX17 and greater than 85% were $FOXA2^+$ at this stage. Base culture medium influenced the efficiency of endoderm induction, as culture in neural basal medium rather than StemPro34 resulted in the generation of EBs with lower percentages of endoderm (supplementary material Fig. S1B). The expansion of the endoderm population was preceded by the transient expression of the primitive streak gene *T*, and accompanied by the upregulation of expression of genes that mark endoderm development, including *SOX17*, goosecoid (GSC) and *FOXA2* (supplementary material Fig. S1C). The generation of highly enriched endoderm is an important first step in the protocol, as induction levels of less than 90% $CXCR4^+CKIT^+$ and 80% $SOX17^+$ cells results in suboptimal hepatic lineage development (data not shown).

Duration of nodal/activin signaling impacts hepatic development

To specify the $CXCR4^+CKIT^+$ population to a hepatic fate, day 6 EBs were dissociated and the cells plated as a monolayer on Matrigel-coated plates in the presence of FGF10 and BMP4 for 48 hours, and then in bFGF and BMP4 for 6 days. As previously demonstrated in mouse and human ESC cultures (Gouon-Evans et al., 2006; Si-Tayeb et al., 2010b), the combination of BMP and FGF signaling was required for optimal hepatic induction under our conditions (supplementary material Fig. S2A). The FGF10/BMP4 step was included as it was found to increase albumin expression in the differentiation cultures (supplementary material Fig. S2B).

Although these induction conditions did lead to the development of albumin-positive cells by day 24 of differentiation (supplementary material Fig. S2C), they were not optimal as the proportion of $SOX17^+$ and $FOXA2^+$ cells within the culture had decreased from more than 90% to ~50% by day 10 (Fig. 2A). As we have previously demonstrated that prolonged activin/nodal signaling promotes endoderm development in mouse ESC differentiation cultures (Gadue et al., 2006), we extended the activin induction step for an additional 2 days prior to the FGF/BMP4 specification step in an attempt to sustain the endoderm population in the human cultures. Extended activin signaling did lead to a significant increase in the proportion of $SOX17^+$ and $FOXA2^+$ cells detected at day 12 (Fig. 2A; supplementary material Fig. S3A). The prolonged activin treatment reduced the total cell number in the

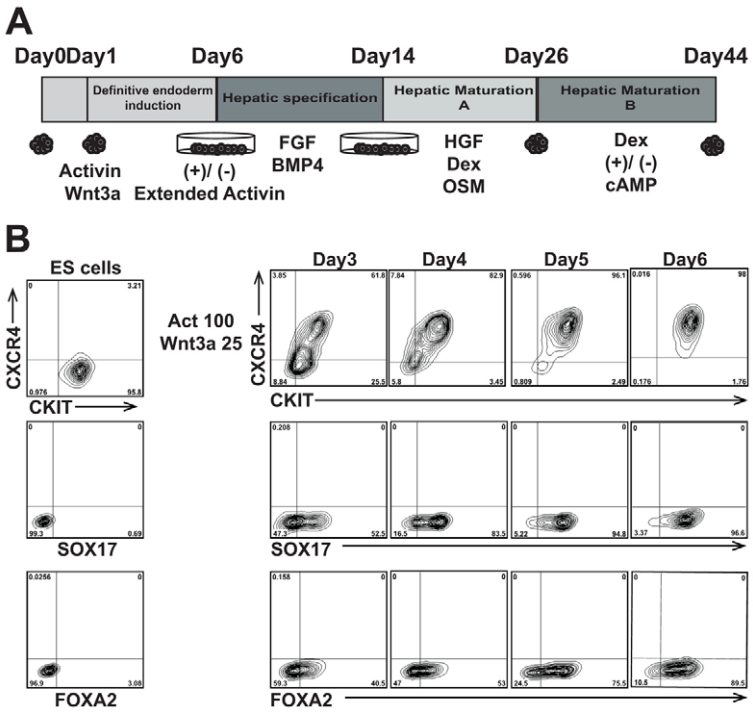

Fig. 1. Endoderm induction in hESC-derived embryoid bodies. (**A**) The differentiation protocol. (**B**) Flow cytometric analyses showing the kinetics of development of the CXCR4$^+$, CKIT$^+$, SOX17$^+$ and FOXA2$^+$ populations in the activin/Wnt3a-induced EBs.

cultures (Fig. 2B), suggesting that these conditions may preferentially support the survival of endodermal cells.

The extended activin culture maintained the CXCR4$^+$CKIT$^+$ population until day 8 (supplementary material Fig. S3B) and resulted in higher levels of expression of genes indicative of hepatic progenitor (hepatoblast) development, including *HEX* (*HHEX* – Human Gene Nomenclature Database), *AFP*, *ALB* and *HNF4A* at day 26 (Fig. 2C). Cultures generated from non-treated CXCR4$^+$CKIT$^+$ endoderm contained contaminating mesoderm, as demonstrated by the expression of *MEOX1*, *MESP1*, *CD31* (*PECAM1* – Human Gene Nomenclature Database) and *CD90* (*THY1* – Human Gene Nomenclature Database), and by the presence of CD90$^+$ cells and CD31$^+$ endothelial cells at day 24 (Fig. 2C,D). Populations derived from the activin-treated endoderm showed reduced expression of the mesoderm genes, had a higher proportion of EPCAM$^+$ cells, no detectable CD31$^+$ cells and a much smaller CD90 population (Fig. 2D). Consistent with these differences, we observed a significantly higher proportion of albumin-positive cells in the treated compared with the non-treated population at day 26 of culture (Fig. 2E,F). The number of AFP-positive cells was not different between the two groups.

Aggregation promotes hepatic maturation

As previous studies have shown that cell aggregation can promote some degree of maturation of hESC-derived hepatic cells (Miki et al., 2011; Nagamoto et al., 2012; Sivertsson et al., 2013; Takayama et al., 2013), we next generated aggregates from the day 26 population (Fig. 3A) and cultured them for 6 days in the presence of HGF, dexamethasone (Dex) and oncostatin M (OSM) to determine whether these conditions would affect maturation of the hepatoblast-like cells in our cultures. Aggregation did increase the expression of a number of genes associated with liver function, including albumin, *CPS1* (carbamonyl-phosphatase synthase 1), *TAT* (tyrosine aminotransferase), *G6P* (glucose 6 phosphatase) and *TDO2* (tryptophan 2,3-dioxygenase) over that observed in monolayer culture. The expression of some (*CYP7A1*, *CYP3A7* and *CYP3A4*) but not all (*CYP1A2* and *CYP2B6*) P450 genes was upregulated by aggregation (Fig. 3C and data not shown). In addition to the different enzyme genes, aggregation also increased the proportion of cells expressing asialo-glycoprotein receptor 1 (ASGR1) a cell-surface marker found on mature hepatocytes (Basma et al., 2009) (Fig. 3D). Immunostaining showed that ASGR1 was detected on albumin$^+$ cells (Fig. 3E). The albumin$^+$ cells in the aggregates also expressed E-cadherin, indicating that they had acquired epithelial characteristics, a property of hepatocytes found in the intact liver (Fig. 3F). The ability to store glycogen, as measured by PAS staining, was not dependent on aggregation, as both monolayer cells and aggregates displayed this capacity (supplementary material Fig. S4). Collectively, these findings show that the simple process of aggregation into 3D structures promotes changes indicative of hepatic maturation.

cAMP signaling induces maturation of hESC-derived hepatocyte-like cells

To further mature the cells, we investigated the role of cAMP signalling, as studies using hepatic cell lines have shown that activation of this pathway induces hepatic gene expression, in part through the induction of the peroxisome proliferator-activated receptor γ co-activator 1α (*PGC1A*; *PPARGC1A* – Human Gene Nomenclature Database), a co-activator that functions together with *HNF4A* to regulate the expression of many genes involved in hepatocyte function (Bell and Michalopoulos, 2006; Arpiainen et al., 2008; Benet et al., 2010; Dankel et al., 2010). Treatment of the aggregates with 8-bromoadenosine-3′,5′-cyclic monophosphate (8-Br-cAMP), a cell-permeable analogue of cAMP, from days 32 to 44 of culture significantly enhanced the expression of *PGC1A* (15-fold), *G6P* (25-fold) and *TAT* (33-fold) but not that of *HNF4A* (Fig. 4A). By contrast, the expression levels of *AFP* and *ALB* were downregulated by 8-Br-cAMP. Flow cytometric analyses confirmed the *AFP* expression analyses and showed a reduction in the number of AFP-positive cells in the 8-Br-cAMP treated aggregates, compared with the non-treated controls. The proportion of ALB-

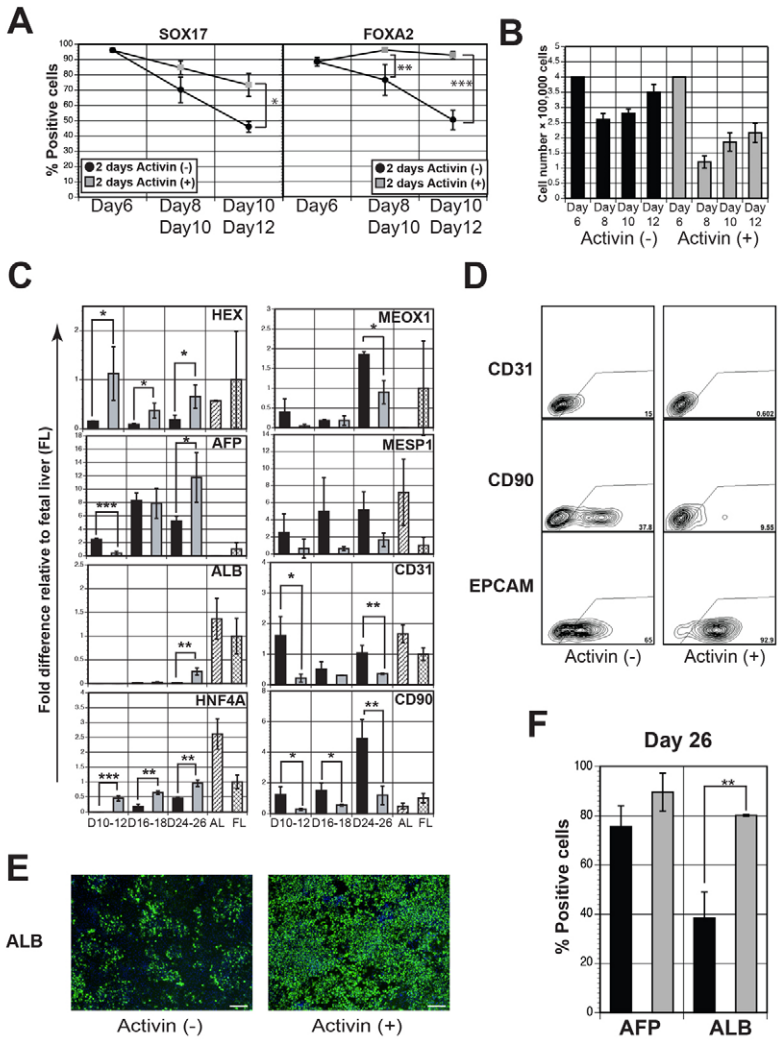

Fig. 2. Duration of nodal/activin signaling impacts hepatic development. (**A**) Intracellular flow cytometric analysis showing the proportion of SOX17$^+$ and FOXA2$^+$ cells in day 6 activin/Wnt3A-induced EBs, as well as in monolayer populations derived from them. The monolayer populations were cultured either directly in the specification medium (–activin) or for 2 days in activin (50 ng/ml) and then in the specification medium (+activin). Populations were analyzed following 2 or 4 days of culture in the specification medium (total days: 8 and 10 for the –activin group; 10 and 12 for the +activin group). Bars represent s.d. of the mean of three independent experiments. (**B**) Total cell number in activin-treated and non-treated monolayer cultures. (**C**) RT-qPCR-based expression analyses of hepatic monolayer populations generated from activin-treated (black bars) and non-treated (gray bars) endoderm. Activin-treated populations (gray bars) were analyzed at days 12, 18 and 26 of total culture, whereas the non-treated population (black bar) was analyzed at days 10, 16 and 24 of culture. Values are determined relative to *TBP* and presented as fold change relative to expression in fetal liver, which is set at 1. AL (adult liver): n=2, AL1, AL2. FL (fetal liver): n=2, FL1, FL2. (**D**) Flow cytometric analysis showing the proportion of CD31$^+$, CD90$^+$ and EPCAM$^+$ cells in monolayer populations derived from activin-treated (day 26) and non-treated (day 24) endoderm. The CD31$^+$ and CD90$^+$ populations were significantly larger in non-treated compared with the treated cultures (CD31, 13.6±2.3% versus 0.49±0.11%, P<0.001; CD90, 41.2±4.7% versus 8.5±1.19%, P<0.001, Student's t-test, n=3). By contrast, a higher proportion of EPCAM$^+$ cells was detected in the population derived from the activin-treated endoderm compared with the population generated from the non-treated cells (EPCAM, 90.7±2.7% versus 56.8±7.3%; P<0.01, n=3). (**E**) Immunostaining analyses showing the proportion of albumin-positive cells in cultures generated from activin-treated (day 26) and non-treated (day 24) endoderm. Albumin is visualized with Alexa 488 (green), nuclei are shown following staining with DAPI (blue). Scale bars: 200 μm. (**F**) Intracellular flow cytometric analyses indicating the proportion of albumin (ALB) and α-fetoprotein (AFP) cells in monolayer cultures generated from activin-treated (gray bars; day 26) and non-treated (black bars; day 24) endoderm. Error bars in all figures represent the s.d. of the mean of three independent experiments. *P<0.05, **P<0.01, ***P<0.001 (Student's t-test; n=3).

positive cells was not reduced despite a decline in mRNA levels (Fig. 4B). These differences could reflect differences in RNA versus protein expression. The addition of 8-Br-cAMP did not impact the structure of the aggregates (supplementary material Fig. S5A) or the viability of the cells (typically >70%) during this culture period.

Immunostaining analyses were consistent with the flow cytometry data and showed that cAMP-treated aggregates expressed similar levels of ALB but lower levels of AFP compared with the non-treated ones (Fig. 4C). The levels of HNF4α protein in both aggregate populations were comparable, confirming the PCR analyses. Albumin secretion by the hESC-derived cells was not impacted by 8-Br-cAMP treatment but was dramatically enhanced by the aggregation step. (Fig. 4D). By contrast, the capacity to take up indocyanine green (ICG), a characteristic of adult hepatocytes (Stieger et al., 2012) was enhanced by cAMP signaling (Fig. 4E).

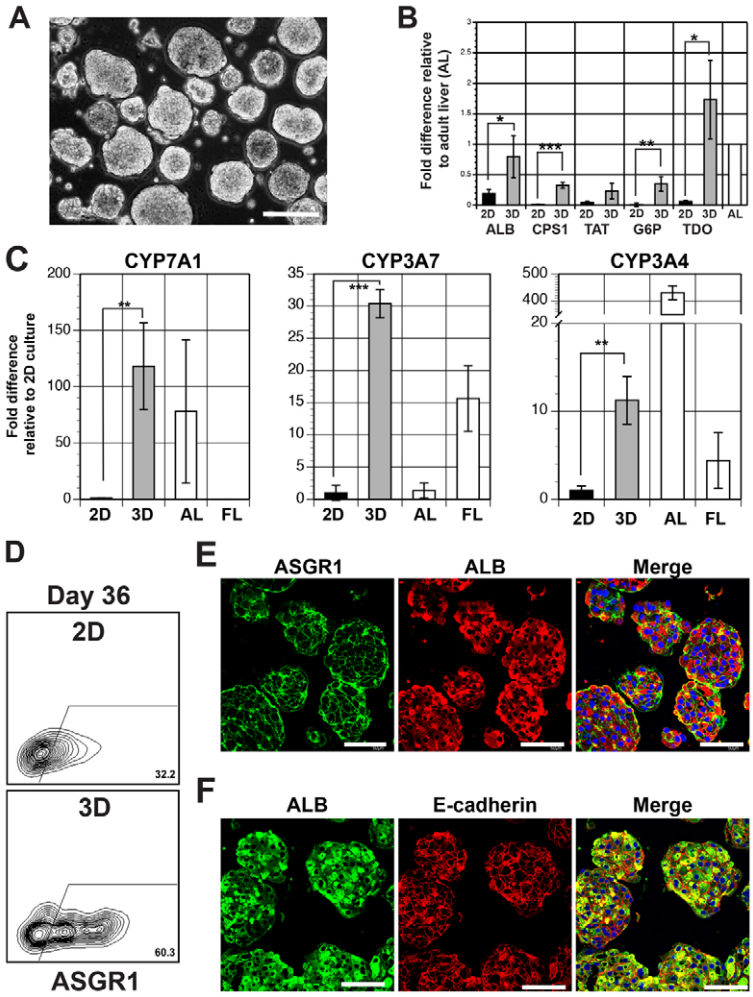

Fig. 3. Aggregation promotes hepatoblast maturation. (**A**) Phase-contrast image of hepatic aggregates at day 28 of culture. Scale bar: 200 μm. (**B**) RT-qPCR based analyses of expression of indicated genes in monolayer (black bar) and 3D aggregate cultures (gray bar) at day 32 of differentiation. Values are determined relative to *TBP* and presented relative to expression in adult liver, which is set at 1. (**C**) RT-qPCR based analysis for *CYP7A1*, *CYP3A7* and *CYP3A4* expression at day 32 of differentiation in monolayer (black bar) and 3D aggregate cultures (gray bar). Values are determined relative to *TBP* and presented as fold change relative to expression in monolayer (2D) cells, which is set at one. AL (adult liver) : n=2, AL1, AL2. FL (fetal liver): n=2, FL1, FL2. (**D**) Flow cytometric analysis showing the proportion of ASGR1 cells in the monolayer (2D) and aggregate (3D) cultures at day 36. The number of ASGR1$^+$ cells was significantly higher in 3D aggregate cultures (2D, 28.8±3.1%; 3D, 64.7±4.26%, P<0.001, n=3). (**E**) Confocal microscopic images of immunostained day 32 aggregates showing co-expression of albumin and ASGR1. Albumin is visualized by Cy3 (red), ASGR1 by Alexa 488 (green) and the nuclei by DAPI (blue). Scale bars: 50 μm. (**F**) Confocal microscopic images of immunostained day 32 aggregates showing co-expression of albumin and E-cadherin. Albumin is visualized by Alexa 488 (green), E-cadherin by Cy3 (red) and the nuclei by DAPI (blue). Scale bars: 50 μm. Error bars in all graphs represent the s.d. of the mean of samples from three independent experiments, *P<0.05, **P<0.01, ***P<0.001, Student's t-test.

Other tissues, such as the pancreas, also express *PGC1A*. However, in contrast to the observed induction in hepatic cells, expression of *PGC1A* was not induced by cAMP signaling in hESC-derived insulin-positive pancreatic cells (supplementary material Fig. S5B), indicating that this response may be tissue specific.

cAMP signaling increases metabolic enzyme activity in hESC-derived hepatocytes

cAMP signaling also induced changes in the expression pattern of key Phase I cytochrome P450 genes, notably a reduction in the levels of expression of the fetal gene *CYP3A7*, and a significant increase in expression of the adult genes *CYP3A4* (2.5-fold), *CYP1A2* (18-fold) and *CYP2B6* (4.7-fold) (Fig. 5A). UGT1A1, an important Phase II enzyme, was also significantly induced (11-fold) by 8-Br-cAMP (Fig. 5A). The inductive effects of cAMP signaling on the P450 genes were observed only in cells in the 3D aggregates, as little increase in expression of *CYP1A2* and *CYP3A4* was detected when it was added to monolayer cultures (Fig. 5B). Expression of *PGC1A* and *TAT* was induced in the monolayer format, likely due to the fact that the promoter regions of these genes contain cAMP-response element binding protein (CREB) sites.

cAMP signaling appeared to be most effective on highly enriched, appropriately patterned cells, as demonstrated by the fact that the levels of induction of *CYP1A2* and *ALB* expression were significantly higher in the aggregates from the extended-activin treated endoderm (+Act) compared with the aggregates from the non-treated endoderm (–Act) (Fig. 5C). To determine whether the changes in gene expression are dependent on continuous signaling, cells induced with 8-Br-cAMP for 6 days and then maintained in the absence of 8-Br-cAMP for the remaining 6 days were compared with those cultured for the entire 12 days in 8-Br-cAMP (Fig. 5D). Expression of *CYP1A2* was maintained following the shorter induction time, demonstrating that the higher levels of expression are not dependent on continuous signaling but rather reflect changes indicative of hepatocyte maturation.

To investigate the functional activity of the P450 enzymes, we determined the ability to metabolize isozyme-selective marker drugs. Additionally, the inducibility of the metabolic activity of two of the key enzymes, CYP1A2 and CYP3A4, was also evaluated. As shown in Fig. 5E, the 8-Br-cAMP-treated cells were able to metabolize the CYP1A2-selective substrate phenacetin. Induction of the cells with lansoprazole for 72 hours resulted in a 3.4-fold increase in this activity. The non-treated (8-Br-cAMP) cells had low levels of activity that were not inducible. Two independent primary hepatocyte samples showed lower or comparable levels of basal metabolic activity, but did display higher levels of induction (18- and 9-fold). CYP3A4 activity was measured by the ability of the cells to metabolize testosterone to 6β-hydroxyl testosterone. As shown in Fig. 5F the 8-Br-cAMP-treated cells displayed this activity. Addition of the CYP3A4 inducer rifampicin increased the activity 2.2-fold, indicating that this enzyme was also inducible in the hESC-derived cells. As observed with CYP1A2, little CYP3A4 activity was detected in the non-induced cells. The primary hepatocytes showed low but significant levels of CYP3A4 induction.

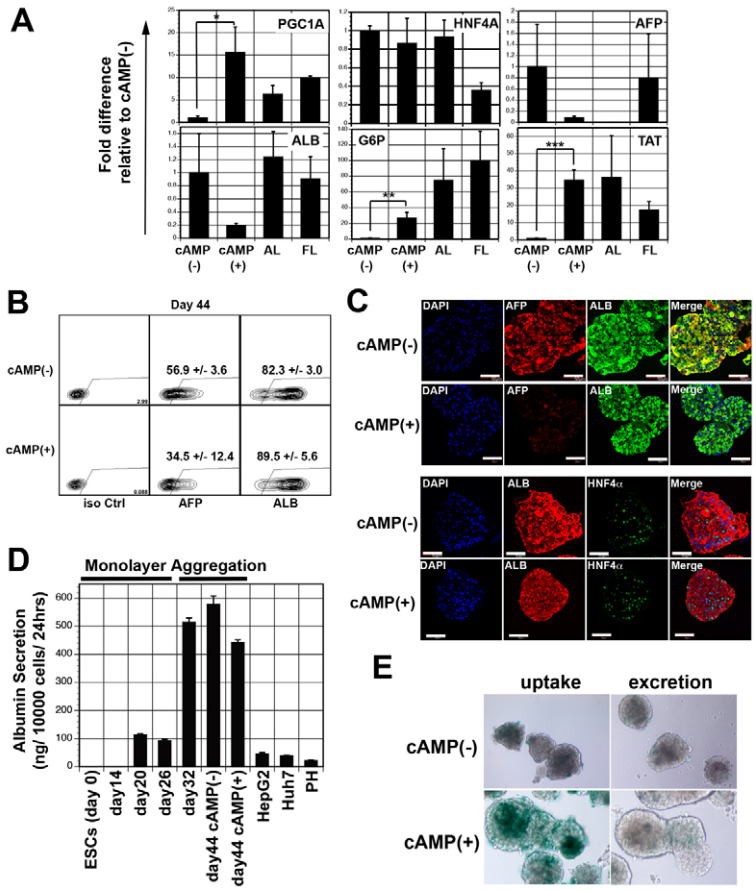

Fig. 4. cAMP induces maturation of hESC-derived hepatocyte-like cells. (**A**) RT-qPCR-based expression analysis of indicated genes in hepatic aggregates cultured in the presence and absence of 8-Br-cAMP. Values are determined relative to *TBP* and presented as fold change relative to expression of the non-treated cells which is set at 1. AL (adult liver): n=2, AL1, AL2. FL (fetal liver): n=2, FL1, FL2. (**B**) Intracellular flow cytometric analysis showing the proportion of α-fetoprotein (AFP)$^+$ and albumin (ALB)$^+$ cells (day 44) in hepatic aggregates cultured in the presence and absence of 8-Br-cAMP. The number of AFP$^+$ cells was significantly lower in the population induced with cAMP compared with the non-induced population (34.5±12.4% versus 56.9±3.6%, P<0.05, mean±s.d., n=3), whereas the proportion of ALB$^+$ cells was higher in the treated population [89.5±5.6% versus 82.3±3.0%, P<0.05 (mean±s.d., n=3)]. (**C**) Confocal microscopic images showing co-expression of ALB and AFP or ALB and HNF4α in day 44 aggregates cultured in the presence and absence of 8-Br-cAMP. In the upper panel, albumin is visualized by Alexa 488 (green), AFP by Cy3 (red) and the nuclei by DAPI (blue). In the lower panel, albumin is visualized by Cy3 (red), HNF4α by Alexa 488 (green) and the nuclei by DAPI (blue). Scale bars: 50 μm. (**D**) The levels of albumin (ALB) secreted by hESC-derived monolayer and aggregate populations, as well as by HepG2 cells, Huh7 cells and cryopreserved hepatocytes (PH, lot OSI). Secretion was detected using an ELISA assay. (**E**) ICG uptake and release by cAMP-treated and non-treated day 44 aggregates. Error bars in all graphs represent the s.d. of the mean of the values from three independent experiments. *P<0.05, **P<0.01, ***P<0.001, Student's t-test,

CYP2B6 activity, as measured by the hydroxylation of bupropion was also detected in the 8-Br-cAMP-treated cells, at levels comparable with those found in primary hepatocytes (Fig. 5G). Analyses of phase II metabolic enzymes, including the arylamine *N*-acetyltransferases NAT2 and/or NAT1 (Fig. 5H) and UDP-glucuronosyltransferase (UGT) (Fig. 5I) revealed activity higher than that of cryopreserved primary cultured hepatocytes, indicating that cAMP signaling induced the upregulation of expression of a broad range of enzymes, consistent with maturation of the population. Together, these observations indicate that cAMP signaling promotes maturation of the hESC-derived hepatocyte-like cells in the 3D aggregates to metabolically functional cells.

Hepatic specification and maturation from other hPSC lines

When induced with the above EB-based protocol, the hESC lines H9 and H1 and the induced pluripotent cell (iPSC) line 38-2 generated populations that contained high frequencies of CKIT$^+$CXCR4$^+$ and CKIT$^+$EPCAM$^+$ cells (Fig. 6A). Differences were, however, observed in the proportion of cells within the EBs that expressed SOX17$^+$ and FOXA2$^+$ (Fig. 6A), indicating that surface marker analysis alone is not sufficient to monitor endoderm development. Extended activin/nodal signaling also improved hepatic development of the CKIT$^+$CXCR4$^+$ population from these hPSC lines; however, the time of treatment necessary to generate significant levels of ALB-positive cells varied between them. Whereas populations consisting of 90% ALB+ cells were obtained following 2 days of activin treatment with H9-derived cells, both H1 and 38-2 cells required 4 days of additional activin signaling to generate populations that contained at least 70% ALB+ cells (Fig. 6B). H9-derived cells at day 26 of differentiation showed a cobblestone morphology very similar to that of cultured hepatocytes (supplementary material Fig. S6B). Both the H9 and 38-2-derived hepatocytes stained with PAS, demonstrating their ability store glycogen (supplementary material Fig. S6C).

Addition of 8-Br-cAMP did induce significant levels of expression of *CYP3A4* (16-fold), *CYP1A2* (100-fold) and *CYP2B6* (10-fold), and the Phase II enzyme UGT1A1 (16-fold) in the H9-derived aggregates (Fig. 6D). 8-Br-cAMP also induced the expression of these enzymes in hiPSC-derived derived aggregates (Fig. 6D); however, in the case of *CYP3A4* the differences were not significant. As observed with the HES2 line, the H9-derived cells possessed that lansoprazole-inducible CYP1A2 activity. H9 and iPSC-derived cells also showed CYP3A4 activity that was inducible with rifampicin. Inducible CYP1A2 activity was not detectable in the iPSC-derived cells, possibly reflecting suboptimal differentiation of this population.

Microarray analyses of cAMP stimulated hepatic populations

To further assess the developmental status of the H9-derived hepatic populations, we carried out a microarray analysis comparing the global expression profiles of the cAMP-induced and non-induced cells with that of cultured (48 hours) primary hepatocytes. A total of 23,038 filtered transcripts were used in the final analysis. A two-way unsupervised hierarchical cluster analysis revealed that the three groups appear as distinct populations (supplementary material Fig. S7). The three cAMP-induced populations were the most similar to one another, whereas the three primary hepatocyte populations showed the most

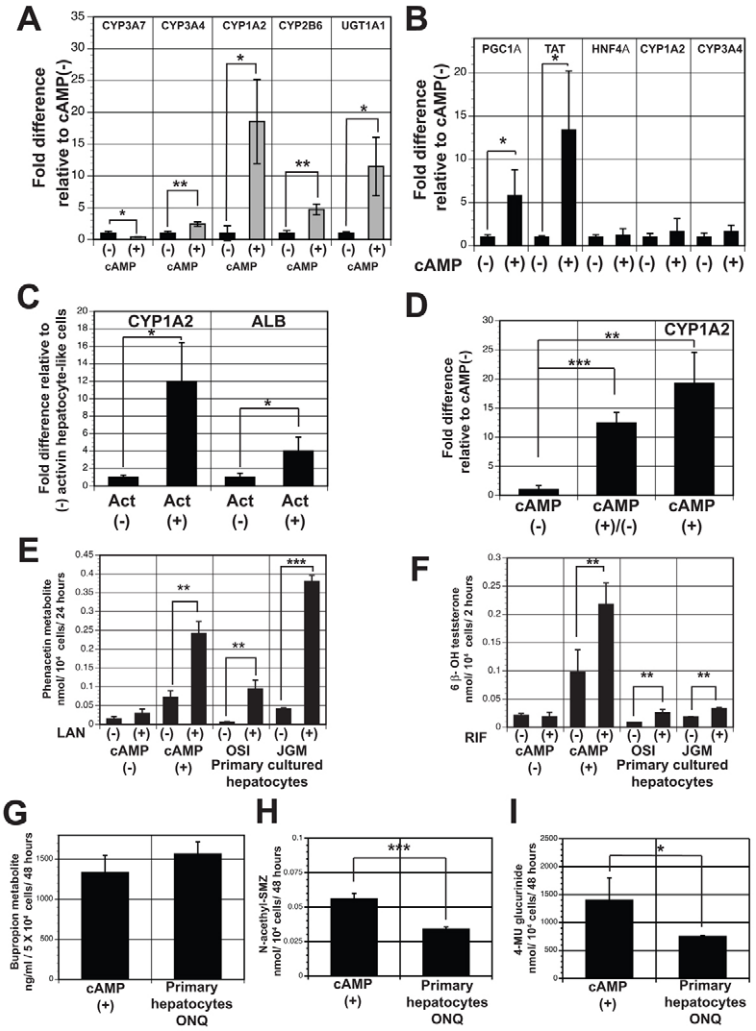

Fig. 5. cAMP increases metabolic enzyme activity in hESC-derived hepatocytes. (**A**) RT-qPCR analysis showing expression of indicated genes in hepatic aggregates (day 44) cultured in the presence and absence of 8-Br-cAMP. Values are determined relative to *TBP* and presented as fold change relative to expression in non-treated cells, which is set at 1. (**B**) RT-qPCR analyses showing expression of indicated genes in untreated (–) and cAMP-treated (+) monolayer populations (day 44). Values are determined relative to *TBP* and presented as fold change relative to expression in non-treated cells, which is set at 1. (**C**) RT-qPCR analyses of *CYP1A2* and *ALB* expression in cAMP-treated aggregates (day 44) generated from non-treated (–Act) or extended activin treated (+Act) endoderm. (**D**) RT-qPCR analyses of *CYP1A2* expression in aggregates cultured for 6 (cAMP+/–) or 12 days in 8-Br-cAMP (cAMP+). (**E**) hESC-derived hepatic cells display lansoprazole (LAN)-inducible CYP1A2 activity *in vitro*. Generation of the *O*-de-ethylated metabolite acetaminophen from phenacetin was monitored by HPLC. Activity is presented per 10,000 cells. Non-induced cells (–) were cultured in 0.1% DMSO-containing medium (n=3). (**F**) hESC-derived hepatic cells display rifampicin (RIF)-inducible CYP3A4 activity *in vitro*. Generation of the 6β-hydroxytestosterone from testosterone was monitored by HPLC. Activity is presented per 10,000 cells. Non-induced cells (–) were cultured in 0.1% DMSO-containing medium (n=3). (**G**) hESC-derived hepatic cells display CYP2B6 activity *in vitro*. Formation of the metabolite *O*-hydroxy-bupropion from bupropion was measured by HPLC. Activity is presented per 50,000 cells (n=3). (**H**) Metabolism of sulfamethazine (SMZ) to *N*-acetylated SMZ indicates the presence of the Phase II enzyme(s) NAT2 and/or NAT1. Activity is presented per 10,000 cells (n=3). (**I**) HPLC analysis showing generation of 4-MU glucuronide (4-MUG) from 4-methylumbelliferone (4-MU) by the cAMP-treated aggregates indicative of total UGT activity. Activity is presented per 10,000 cells (n=3). Error bars in all graphs represent the s.d. of the mean of samples from three independent experiments. **P*<0.05, ***P*<0.01, ****P*<0.001, Student's *t*-test. OSI, JGM and ONQ are three different lots of cultured primary hepatocytes.

divergent expression patterns. A FDR corrected ANOVA (q<0.05) identified 784 transcripts that showed the most statistically significant variability across all three sample groups. A hierarchically clustered visualization of these data identified clusters of highly expressed transcripts in each of the biological groups (Fig. 7A). These clusters consisted of 181 transcripts in the primary hepatocytes, (purple bar) 106 transcripts in the 8-Br-cAMP-induced cells (yellow bar) and 80 transcripts (blue bar) in the non-treated cells (supplementary material Table S2). Genes enriched in 8-Br-cAMP-induced cells included most of the key P450 enzymes, those involved in different aspects of liver function (including gluconeogenesis, glucose homeostasis and lipid metabolism) and those involved in mitochondria function, such as carnitine palmitoyltransferase 1A (CPT1A) and PTEN induced putative kinase 1 (PINK1) [supplementary material Table S2 (q<0.1), Table S11]. The cluster expressed at highest levels in the primary hepatocytes consisted of immune system, inflammatory-related and MHC genes (supplementary material Tables S2, S9, S10). The cluster detected in the non-induced hESC-derived cells did not contain any enriched gene ontology categories.

For a more detailed comparison of the populations, we next analyzed selected sets of transcripts that included a subset of Phase I and II drug metabolizing enzymes, transporters, coagulation factors, lipoproteins, nuclear receptors and transcription factors and general liver enzymes, and other functional molecules (Fig. 7B). The complete gene lists with fold differences in expression are provided in supplementary material Tables S2-S6. Analyses of these data revealed that many of the genes were expressed at comparable levels in the 8-Br-cAMP-treated hESC-derived cells and the primary hepatocytes. Select genes in each category were expressed at significantly higher levels in the 8-Br-cAMP-treated cells compared with the untreated cells or the primary hepatocytes. These include the Phase I enzymes *CYP1A2* and *CYP3A4*; the Phase II enzyme *SULT2A1*; *ASGR1*, *ALB* and the transporter *SLCO1B1*; and the general liver enzymes *TAT*, *G6P* and *TDO2*.

RT-qPCR analyses showed that the levels of *CYP1A2*, *CYP3A4*, *CYP2B6* and *UGT1A1* were significantly higher in 8-Br-cAMP treated cells than in the primary cultured hepatocytes (Fig. 7C), confirming the findings from the microarray analyses. Comparison of the hESC-derived cells to the adult liver revealed levels of *CYP1A2*, *CYP3A4*, *CYP2B6*, *CYP2C9* and *UGT1A1* at 6.8±1.4%, 26.5±5.01%, 11±1.6%, 26.3±5.8% and 82.3±14.5%, respectively, of the levels detected in the intact tissue. Other genes, such as *G6P* and *TAT*, were expressed at similar levels to those found in the adult liver. The levels of expression in the cultured hepatocytes were substantially lower than the levels in the adult liver samples, reflecting the loss of metabolic activity of cultured hepatocytes. Taken together, these findings demonstrate that induction of hepatoblast-stage aggregates with cAMP results in global expression changes indicative of hepatocyte maturation.

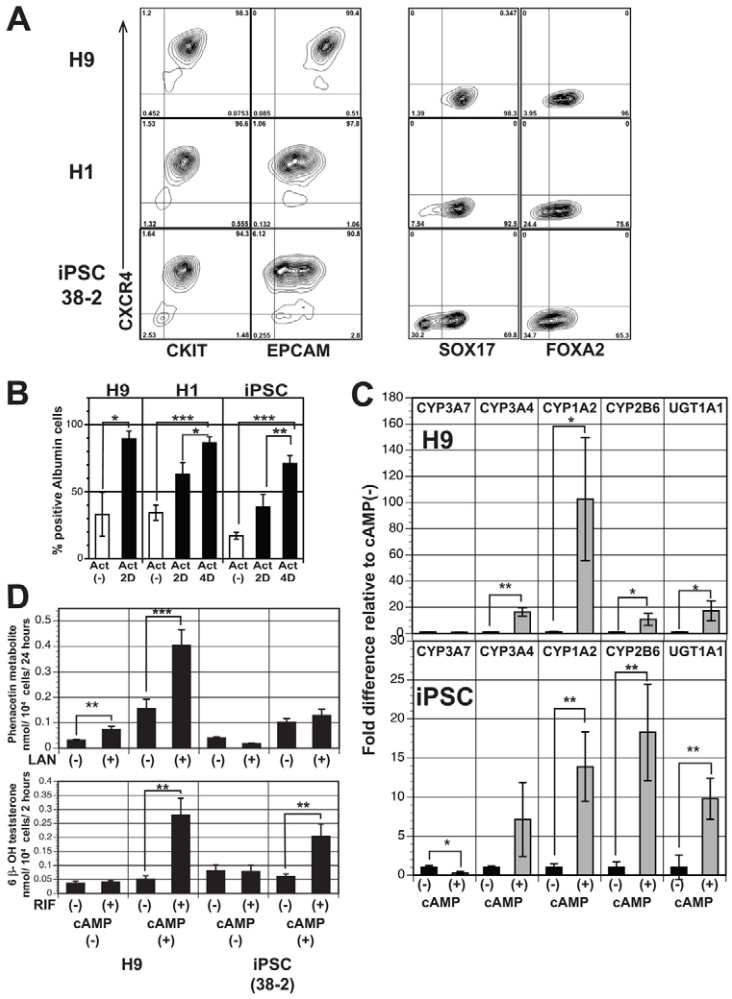

Fig. 6. Hepatic specification and maturation from other hPSCs lines. (**A**) Flow cytometric analyses showing the proportion of CXCR4$^+$, CKIT$^+$, EPCAM$^+$, SOX17$^+$ and FOXA2$^+$ cells in activin/Wnt3a-induced day 6 EBs generated from H9 hESCs, H1 hESCs and 38-2 iPSCs. (**B**) Intracellular flow cytometric analyses showing the number of ALB-positive cells generated from the different hPSC lines [no activin (–), day 24; 2-day activin, day 26; 4-day activin, day 28 of differentiation]. (**C**) RT-qPCR analyses showing expression of indicated genes in H9- and iPSC (38-2)-derived hepatic aggregates (day 44) cultured in the presence and absence of 8-Br-cAMP. Values are determined relative to *TBP* and presented as fold change relative to expression in non-treated cells, which is set at 1. (**D**) CYP1A2 and CYP3A4 activity in hepatic cells derived from H9 hESCs and 38-2 iPS. Activity is presented per 10,000 cells. Non-induced cells (–) were cultured in 0.1% DMSO-containing medium (n=3). Primary hepatocyte controls are the same as in Fig. 5E,F. Error bars in all graphs represent the s.d. of the mean of the values from three independent experiments, *P<0.05, **P<0.01, ***P<0.001, Student's t-test.

DISCUSSION

Previous studies have shown that it is possible to generate immature hepatic lineage cells from both hESCs and hiPSCs using staged protocols designed to recapitulate crucial developmental steps in the embryo (Cai et al., 2007; Hay et al., 2008; Si-Tayeb et al., 2010b; Touboul et al., 2010; Funakoshi et al., 2011; Kajiwara et al., 2012). The success of these studies reflects the fact that the pathways controlling the early stages of differentiation are reasonably well defined. In this report, we extended the differentiation protocol to provide insights into pathways that regulate maturation of hESC-derived hepatocyte-like cells and demonstrate that the combination of 3D aggregation and cAMP signaling play a pivotal role at this stage of development. We also show that the duration of activin/nodal signaling following endoderm induction is crucial for the generation of an enriched progenitor population that can respond to cAMP. With these manipulations, it is possible to routinely generate hESC-derived populations that display measurable levels of Phase I and II metabolic enzymes and gene expression profiles indicative of hepatocyte maturation.

Our expression analyses showed that the cAMP-induced cells expressed higher levels of metabolic genes and other genes involved in hepatocyte function than found in cultured primary hepatocytes. Comparison with adult liver revealed that the hESC-derived cells had levels of the Phase I enzyme genes in the range of 7-27% and of the Phase II gene *UGT1A1* at 82% of those found in the adult tissue. Several previous studies have reported the development of hPSC-derived hepatocytes that express some P450 enzyme activity (Duan et al., 2010; Hay et al., 2011; Takayama et al., 2011; Nagamoto et al., 2012; Takayama et al., 2012; Takayama et al., 2013). Duan et al. (Duan et al., 2010) were the first to successfully generate cells that had *CYP1A2*, *CYP3A4*, *CYP2C9* and *CYP2D6* enzyme activities comparable with those found in primary hepatocytes. These findings were encouraging as they demonstrated that it is possible to derive metabolically active cells from hESCs. This study did not, however, provide any insights into the pathways that promote maturation or show that the approach was applicable to different cell lines. More recent studies have shown that culture on specific polymers (Hay et al., 2011), culture as 3D aggregates (Sivertsson et al., 2013) or the combination of enforced expression of key transcription factors together with 3D aggregation (Takayama et al., 2013) promote the development hPSC-derived hepatocytes that express CYP genes. Of these, only two showed inducible CYP activity. Hay et al. reported general CYP3A activity, whereas Takayama and colleagues showed rifampicin-inducible CYP3A4 activity in iPSC-derived cells. Although the cells in the later study display Phase I and II gene expression profiles at levels similar to those in primary hepatocytes, this approach does have the drawback in that the development of the cells is dependent on viral transduction of different transcription factors.

The observation that sustained activin/nodal signaling within the CXCR4$^+$CKIT$^+$ population is crucial for the generation of mature

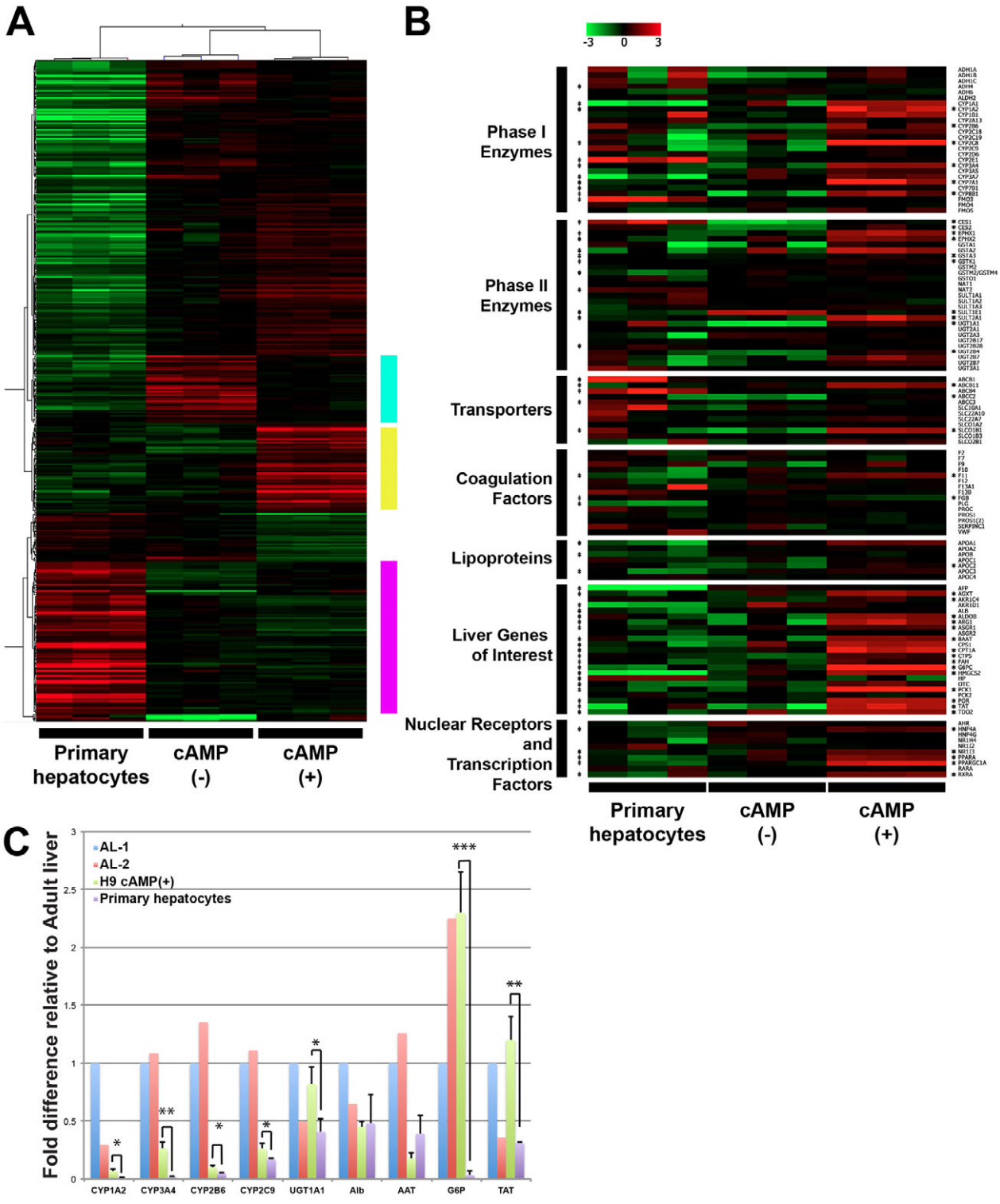

Fig. 7. Microarray analyses comparing primary hepatocytes with non-treated and cAMP-treated hESC-derived hepatic populations. (**A**) Heat map summarizing expression of 784 transcripts that showed the most statistically significant variability across the sample groups. The bars on the right indicate clusters of transcripts highly expressed in each of the biological groups. (**B**) Heat map showing expression of selected transcripts for each of the indicated categories. Asterisks on the right indicate those genes that are expressed at significantly higher levels in the cAMP-treated hESC-derived cells compared with primary hepatocytes, whereas markings on the left indicate those that are significantly higher in the cAMP-treated hESC-derived cells compared with non-treated hESC population. (**C**) RT-qPCR analyses comparing expression levels of *CYP1A2*, *CYP3A4*, *CYP2B6*, *CYP2C9*, *UGT1A1*, *ALB*, a1-anti trypsin (*AAT*), *G6P* and *TAT* expression in day 44 H9-derived cAMP-treated aggregates (day 44) with those in adult liver and cultured primary hepatocytes. Values are determined relative to *TBP* and presented as fold change relative to expression in the adult liver sample 1 (AL1), which is set at 1. AL1: total human adult liver RNA. AL2: total human adult liver RNA. Error bars in all graphs represent the s.d. of the mean of the values from three independent experiments. **P*<0.05, ***P*<0.01, ****P*<0.001, Student's *t*-test.

hepatocytes highlights the importance of appropriate manipulation of early-stage cells for the efficient generation of mature cells. The effect of extended activin/nodal signaling between days 6 and 8 of differentiation (for HES2 cells) is striking, as it dramatically impacted gene expression patterns and the proportion of albumin-positive cells detected at day 26 of culture. Most importantly, this step promoted the development of a population of hepatic cells that, in response to cAMP, mature to give rise to metabolically functioning hepatocytes. This additional signaling step is not compensation for poor endoderm induction, as the day 6 EB target population consisted of greater than 95% $CXCR4^+CKIT^+EPCAM^+SOX17^+$ cells. Rather, it appears to reduce contaminating mesoderm-derivatives ($CD90^+$ and $CD31^+$ cells), possibly due to the inability of activin to promote their survival in the absence of BMP or FGF. The extended activin step may also play a role in endoderm patterning, as previous studies have shown that the duration of activin/nodal signaling does influence lineage specification from hESC-derived endoderm (Green et al., 2011; Nostro et al., 2011; Spence et al., 2011).

The maturation stage of our protocol involves two distinct, but interdependent, steps. The first is the generation of 3D aggregates. As shown in previous studies (Miki et al., 2011; Sivertsson et al., 2013) and in the work reported here, culture of hPSC-derived hepatic cells as 3D aggregates leads to the upregulation of expression of a wide range of genes involved in different aspects of liver function. Aggregation alone, however, does not appear to promote maturation of the population to the stage at which the cells have functional levels of enzyme activity. Development of such cells is dependent on additional maturation signals, one of which we have shown to be cAMP. Importantly, the 3D aggregation step does induce maturation to the stage at which the cells can respond to cAMP. The mechanism by which aggregation promotes this differentiation step is currently not known, but could be related to enhanced cellular interactions and the generation of polarized epithelial cells that mimic the morphology of the hepatocytes within the liver.

The second step of our maturation strategy is the activation of the cAMP pathway within the 3D aggregates that results in broad changes in gene expression indicative of maturation of the hepatic lineage. Notable among these changes was the upregulation of expression of two key CYP genes, *CYP1A2* and *CYP3A4*, that are not expressed in the liver until after birth and function to metabolize many of the clinically relevant drugs (Hines and McCarver, 2002). These changes were indicative of function as the cAMP-treated cells displayed inducible CYP1A2 and CYP3A enzyme activity. cAMP and *PGC1A* have been shown to regulate gene expression patterns in the liver *in vivo*. For example, under conditions of fasting, cAMP levels are upregulated, resulting in the rapid induction of *PGC1A*, a co-factor for *HNF4A* (Iordanidou et al., 2005; Bell and Michalopoulos, 2006) that plays a crucial role in liver metabolism through the control of Phase I and Phase II drug-metabolizing enzyme activities, glucose metabolism and lipid production (Parviz et al., 2003; Rhee et al., 2003; Odom et al., 2004). Expression of *PGC1A* is also dramatically upregulated in mouse liver immediately after birth (Lin et al., 2003) possibly to promote maturation of the neonatal hepatocytes. Through the upregulation of *PGC1A* expression, the effects of cAMP signaling on the hPSC-derived hepatoblasts may be recapitulating the change observed in the liver during fasting and/or in hepatocyte lineage at birth, resulting the generation of cells that display many features of mature cells.

In summary, our findings have, for the first time, defined crucial steps that promote the maturation of hepatic lineage cells from hPSCs resulting the generation of cells that display functional properties of hepatocytes. The development of metabolically functional cells is an important end point that will enable the routine production of hPSC-derived hepatocyte-like cells for drug metabolism analyses in the pharmaceutical industry. The cAMP-induced cells also provide an ideal candidate population for the development of bio-artificial liver devices and ultimately for transplantation for cell replacement therapy for the treatment of liver disease. Both the drug metabolism and therapeutic applications will require scalable production that enables the routine generation of large numbers of these cells. Current efforts are aimed at optimizing expansion strategies at different stages of the protocol.

Acknowledgements
We thank members of the G.K. laboratory for discussion and critical reading of the manuscript; M. C. Nostro and F. Sarangi for generating the islet-like cells from hESCs; G. Daley (Harvard Medical School, Boston) for providing the human iPSC line (38-2); S. C. Strom for providing the RNA samples of isolated primary human hepatocytes; and R. Snodgrass for discussion and suggestions.

Funding
This work was supported by funding from VistaGen Therapeutics (San Francisco) and by a grant [SCN 12091] from the Canadian Stem Cell Network (Canada) to G.K., R.F.T., R.R.L. and D.M.G.

Competing interests statement
The authors declare no competing financial interests.

Author contributions
S.O. and G.K. designed the study and wrote the paper. S.O., J.S., M.O. and M.N. designed and carried out the experiments and analyzed the data. C.V. performed microarray experiment and analyzed the data. K.S.S., S.W., L.T., C.G., E.H., Z.B., R.R.L., R.F.T. and D.M.G. designed and performed the drug metabolism assay, and analyzed the data.

Supplementary material
Supplementary material available online at
http://dev.biologists.org/lookup/suppl/doi:10.1242/dev.090266/-/DC1

References

Arpiainen, S., Järvenpää, S. M., Manninen, A., Viitala, P., Lang, M. A., Pelkonen, O. and Hakkola, J. (2008). Coactivator PGC-1alpha regulates the fasting inducible xenobiotic-metabolizing enzyme CYP2A5 in mouse primary hepatocytes. *Toxicol. Appl. Pharmacol.* **232**, 135-141.

Basma, H., Soto-Gutiérrez, A., Yannam, G. R., Liu, L., Ito, R., Yamamoto, T., Ellis, E., Carson, S. D., Sato, S., Chen, Y. et al. (2009). Differentiation and transplantation of human embryonic stem cell-derived hepatocytes. *Gastroenterology* **136**, 990-999.

Bell, A. W. and Michalopoulos, G. K. (2006). Phenobarbital regulates nuclear expression of HNF-4alpha in mouse and rat hepatocytes independent of CAR and PXR. *Hepatology* **44**, 186-194.

Benet, M., Lahoz, A., Guzmán, C., Castell, J. V. and Jover, R. (2010). CCAAT/enhancer-binding protein alpha (C/EBPalpha) and hepatocyte nuclear factor 4alpha (HNF4alpha) synergistically cooperate with constitutive androstane receptor to transactivate the human cytochrome P450 2B6 (CYP2B6) gene: application to the development of a metabolically competent human hepatic cell model. *J. Biol. Chem.* **285**, 28457-28471.

Benjamini, Y., Drai, D., Elmer, G., Kafkafi, N. and Golani, I. (2001). Controlling the false discovery rate in behavior genetics research. *Behav. Brain Res.* **125**, 279-284.

Byers, J., Bachmann, K., Eng, H., Katta, A., White, D., Ghosh, R., Hewitt, N. J., Silber, P. and Chen, G. (2007). An estimate of the number of hepatocyte donors required to provide reasonable estimates of human hepatic clearance from in vitro experiments. *Drug Metab. Lett.* **1**, 91-95.

Cai, J., Zhao, Y., Liu, Y., Ye, F., Song, Z., Qin, H., Meng, S., Chen, Y., Zhou, R., Song, X. et al. (2007). Directed differentiation of human embryonic stem cells into functional hepatic cells. *Hepatology* **45**, 1229-1239.

Chen, Y. F., Tseng, C. Y., Wang, H. W., Kuo, H. C., Yang, V. W. and Lee, O. K. (2012). Rapid generation of mature hepatocyte-like cells from human induced pluripotent stem cells by an efficient three-step protocol. *Hepatology* **55**, 1193-1203.

Dankel, S. N., Hoang, T., Flågeng, M. H., Sagen, J. V. and Mellgren, G. (2010). cAMP-mediated regulation of HNF-4alpha depends on the level of coactivator PGC-1alpha. *Biochim. Biophys. Acta* **1803**, 1013-1019.

Duan, Y., Catana, A., Meng, Y., Yamamoto, N., He, S., Gupta, S., Gambhir, S. S. and Zern, M. A. (2007). Differentiation and enrichment of hepatocyte-like cells from human embryonic stem cells in vitro and in vivo. *Stem Cells* **25**, 3058-3068.

Duan, Y., Ma, X., Zou, W., Wang, C., Bahbahan, I. S., Ahuja, T. P., Tolstikov, V. and Zern, M. A. (2010). Differentiation and characterization of metabolically functioning hepatocytes from human embryonic stem cells. *Stem Cells* **28**, 674-686.

Funakoshi, N., Duret, C., Pascussi, J. M., Blanc, P., Maurel, P., Daujat-Chavanieu, M. and Gerbal-Chaloin, S. (2011). Comparison of hepatic-like cell production from human embryonic stem cells and adult liver progenitor cells: CAR transduction activates a battery of detoxification genes. *Stem Cell Rev.* **7**, 518-531.

Gadue, P., Huber, T. L., Paddison, P. J. and Keller, G. M. (2006). Wnt and TGF-beta signaling are required for the induction of an in vitro model of primitive streak formation using embryonic stem cells. *Proc. Natl. Acad. Sci. USA* **103**, 16806-16811.

Gagné, J. F., Montminy, V., Belanger, P., Journault, K., Gaucher, G. and Guillemette, C. (2002). Common human UGT1A polymorphisms and the altered metabolism of irinotecan active metabolite 7-ethyl-10-hydroxycamptothecin (SN-38). *Mol. Pharmacol.* **62**, 608-617.

Gebhardt, R., Hengstler, J. G., Müller, D., Glöckner, R., Buenning, P., Laube, B., Schmelzer, E., Ullrich, M., Utesch, D., Hewitt, N. et al. (2003). New hepatocyte in vitro systems for drug metabolism: metabolic capacity and recommendations for application in basic research and drug development, standard operation procedures. *Drug Metab. Rev.* **35**, 145-213.

Gouon-Evans, V., Boussemart, L., Gadue, P., Nierhoff, D., Koehler, C. I., Kubo, A., Shafritz, D. A. and Keller, G. (2006). BMP-4 is required for hepatic specification of mouse embryonic stem cell-derived definitive endoderm. *Nat. Biotechnol.* **24**, 1402-1411.

Grant, D. M., Blum, M., Beer, M. and Meyer, U. A. (1991). Monomorphic and polymorphic human arylamine N-acetyltransferases: a comparison of liver isozymes and expressed products of two cloned genes. *Mol. Pharmacol.* **39**, 184-191.

Green, M. D., Chen, A., Nostro, M. C., d'Souza, S. L., Schaniel, C., Lemischka, I. R., Gouon-Evans, V., Keller, G. and Snoeck, H. W. (2011). Generation of anterior foregut endoderm from human embryonic and induced pluripotent stem cells. *Nat. Biotechnol.* **29**, 267-272.

Guillouzo, A. (1998). Liver cell models in in vitro toxicology. *Environ. Health Perspect.* **106 Suppl. 2**, 511-532.

Hay, D. C., Fletcher, J., Payne, C., Terrace, J. D., Gallagher, R. C., Snoeys, J., Black, J. R., Wojtacha, D., Samuel, K., Hannoun, Z. et al. (2008). Highly efficient differentiation of hESCs to functional hepatic endoderm requires ActivinA and Wnt3a signaling. *Proc. Natl. Acad. Sci. USA* **105**, 12301-12306.

Hay, D. C., Pernagallo, S., Diaz-Mochon, J. J., Medine, C. N., Greenhough, S., Hannoun, Z., Schrader, J., Black, J. R., Fletcher, J., Dalgetty, D. et al. (2011). Unbiased screening of polymer libraries to define novel substrates for functional hepatocytes with inducible drug metabolism. *Stem Cell Res.* **6**, 92-102.

Hewitt, N. J., Lechón, M. J., Houston, J. B., Hallifax, D., Brown, H. S., Maurel, P., Kenna, J. G., Gustavsson, L., Lohmann, C., Skonberg, C. et al. (2007). Primary hepatocytes: current understanding of the regulation of metabolic enzymes and transporter proteins, and pharmaceutical practice for the use of hepatocytes in metabolism, enzyme induction, transporter, clearance, and hepatotoxicity studies. *Drug Metab. Rev.* **39**, 159-234.

Hines, R. N. and McCarver, D. G. (2002). The ontogeny of human drug-metabolizing enzymes: phase I oxidative enzymes. *J. Pharmacol. Exp. Ther.* **300**, 355-360.

Iordanidou, P., Aggelidou, E., Demetriades, C. and Hadzopoulou-Cladaras, M. (2005). Distinct amino acid residues may be involved in coactivator and ligand interactions in hepatocyte nuclear factor-4alpha. *J. Biol. Chem.* **280**, 21810-21819.

Kajiwara, M., Aoi, T., Okita, K., Takahashi, R., Inoue, H., Takayama, N., Endo, H., Eto, K., Toguchida, J., Uemoto, S. et al. (2012). Donor-dependent variations in hepatic differentiation from human-induced pluripotent stem cells. *Proc. Natl. Acad. Sci. USA* **109**, 12538-12543.

Kennedy, M., D'Souza, S. L., Lynch-Kattman, M., Schwantz, S. and Keller, G. (2007). Development of the hemangioblast defines the onset of hematopoiesis in human ES cell differentiation cultures. *Blood* **109**, 2679-2687.

Klipper-Aurbach, Y., Wasserman, M., Braunspiegel-Weintrob, N., Borstein, D., Peleg, S., Assa, S., Karp, M., Benjamini, Y., Hochberg, Y. and Laron, Z. (1995). Mathematical formulae for the prediction of the residual beta cell function during the first two years of disease in children and adolescents with insulin-dependent diabetes mellitus. *Med. Hypotheses* **45**, 486-490.

Kostrubsky, V. E., Ramachandran, V., Venkataramanan, R., Dorko, K., Esplen, J. E., Zhang, S., Sinclair, J. F., Wrighton, S. A. and Strom, S. C. (1999). The use of human hepatocyte cultures to study the induction of cytochrome P-450. *Drug Metab. Dispos.* **27**, 887-894.

Lin, J., Tarr, P. T., Yang, R., Rhee, J., Puigserver, P., Newgard, C. B. and Spiegelman, B. M. (2003). PGC-1beta in the regulation of hepatic glucose and energy metabolism. *J. Biol. Chem.* **278**, 30843-30848.

Loboz, K. K., Gross, A. S., Ray, J. and McLachlan, A. J. (2005). HPLC assay for bupropion and its major metabolites in human plasma. *J. Chromatogr. B Analyt. Technol. Biomed. Life Sci.* **823**, 115-121.

Miki, T., Ring, A. and Gerlach, J. (2011). Hepatic differentiation of human embryonic stem cells is promoted by three-dimensional dynamic perfusion culture conditions. *Tissue Eng. Part C Methods* **17**, 557-568.

Nagamoto, Y., Tashiro, K., Takayama, K., Ohashi, K., Kawabata, K., Sakurai, F., Tachibana, M., Hayakawa, T., Furue, M. K. and Mizuguchi, H. (2012). The promotion of hepatic maturation of human pluripotent stem cells in 3D co-culture using type I collagen and Swiss 3T3 cell sheets. *Biomaterials* **33**, 4526-4534.

Nostro, M. C., Sarangi, F., Ogawa, S., Holtzinger, A., Corneo, B., Li, X., Micallef, S. J., Park, I. H., Basford, C., Wheeler, M. B. et al. (2011). Stage-specific signaling through TGFβ family members and WNT regulates patterning and pancreatic specification of human pluripotent stem cells. *Development* **138**, 861-871.

Odom, D. T., Zizlsperger, N., Gordon, D. B., Bell, G. W., Rinaldi, N. J., Murray, H. L., Volkert, T. L., Schreiber, J., Rolfe, P. A., Gifford, D. K. et al. (2004). Control of pancreas and liver gene expression by HNF transcription factors. *Science* **303**, 1378-1381.

Parviz, F., Matullo, C., Garrison, W. D., Savatski, L., Adamson, J. W., Ning, G., Kaestner, K. H., Rossi, J. M., Zaret, K. S. and Duncan, S. A. (2003). Hepatocyte nuclear factor 4alpha controls the development of a hepatic epithelium and liver morphogenesis. *Nat. Genet.* **34**, 292-296.

Rhee, J., Inoue, Y., Yoon, J. C., Puigserver, P., Fan, M., Gonzalez, F. J. and Spiegelman, B. M. (2003). Regulation of hepatic fasting response by PPARgamma coactivator-1alpha (PGC-1): requirement for hepatocyte nuclear factor 4alpha in gluconeogenesis. *Proc. Natl. Acad. Sci. USA* **100**, 4012-4017.

Roymans, D., Van Looveren, C., Leone, A., Parker, J. B., McMillian, M., Johnson, M. D., Koganti, A., Gilissen, R., Silber, P., Mannens, G. et al. (2004). Determination of cytochrome P450 1A2 and cytochrome P450 3A4 induction in cryopreserved human hepatocytes. *Biochem. Pharmacol.* **67**, 427-437.

Si-Tayeb, K., Lemaigre, F. P. and Duncan, S. A. (2010a). Organogenesis and development of the liver. *Dev. Cell* **18**, 175-189.

Si-Tayeb, K., Noto, F. K., Nagaoka, M., Li, J., Battle, M. A., Duris, C., North, P. E., Dalton, S. and Duncan, S. A. (2010b). Highly efficient generation of human hepatocyte-like cells from induced pluripotent stem cells. *Hepatology* **51**, 297-305.

Sivertsson, L., Synnergren, J., Jensen, J., Björquist, P. and Ingelman-Sundberg, M. (2013). Hepatic differentiation and maturation of human embryonic stem cells cultured in a perfused three-dimensional bioreactor. *Stem Cells Dev.* **22**, 581-594.

Spence, J. R., Mayhew, C. N., Rankin, S. A., Kuhar, M. F., Vallance, J. E., Tolle, K., Hoskins, E. E., Kalinichenko, V. V., Wells, S. I., Zorn, A. M. et al. (2011). Directed differentiation of human pluripotent stem cells into intestinal tissue in vitro. *Nature* **470**, 105-109.

Stieger, B., Heger, M., de Graaf, W., Paumgartner, G. and van Gulik, T. (2012). The emerging role of transport systems in liver function tests. *Eur. J. Pharmacol.* **675**, 1-5.

Sullivan, G. J., Hay, D. C., Park, I. H., Fletcher, J., Hannoun, Z., Payne, C. M., Dalgetty, D., Black, J. R., Ross, J. A., Samuel, K. et al. (2010). Generation of functional human hepatic endoderm from human induced pluripotent stem cells. *Hepatology* **51**, 329-335.

Takayama, K., Inamura, M., Kawabata, K., Tashiro, K., Katayama, K., Sakurai, F., Hayakawa, T., Furue, M. K. and Mizuguchi, H. (2011). Efficient and directive generation of two distinct endoderm lineages from human ESCs and iPSCs by differentiation stage-specific SOX17 transduction. *PLoS ONE* **6**, e21780.

Takayama, K., Inamura, M., Kawabata, K., Katayama, K., Higuchi, M., Tashiro, K., Nonaka, A., Sakurai, F., Hayakawa, T., Furue, M. K. et al. (2012). Efficient generation of functional hepatocytes from human embryonic stem cells and induced pluripotent stem cells by HNF4alpha transduction. *Mol. Ther.* **20**, 127-137.

Takayama, K., Kawabata, K., Nagamoto, Y., Kishimoto, K., Tashiro, K., Sakurai, F., Tachibana, M., Kanda, K., Hayakawa, T., Furue, M. K. et al. (2013). 3D spheroid culture of hESC/hiPSC-derived hepatocyte-like cells for drug toxicity testing. *Biomaterials* **34**, 1781-1789.

Touboul, T., Hannan, N. R., Corbineau, S., Martinez, A., Martinet, C., Branchereau, S., Mainot, S., Strick-Marchand, H., Pedersen, R., Di Santo, J. et al. (2010). Generation of functional hepatocytes from human embryonic stem cells under chemically defined conditions that recapitulate liver development. *Hepatology* **51**, 1754-1765.

Zhang, F. and Chen, J. Y. (2011). HOMER: a human organ-specific molecular electronic repository. *BMC Bioinformatics* **12 Suppl. 10**, S4.

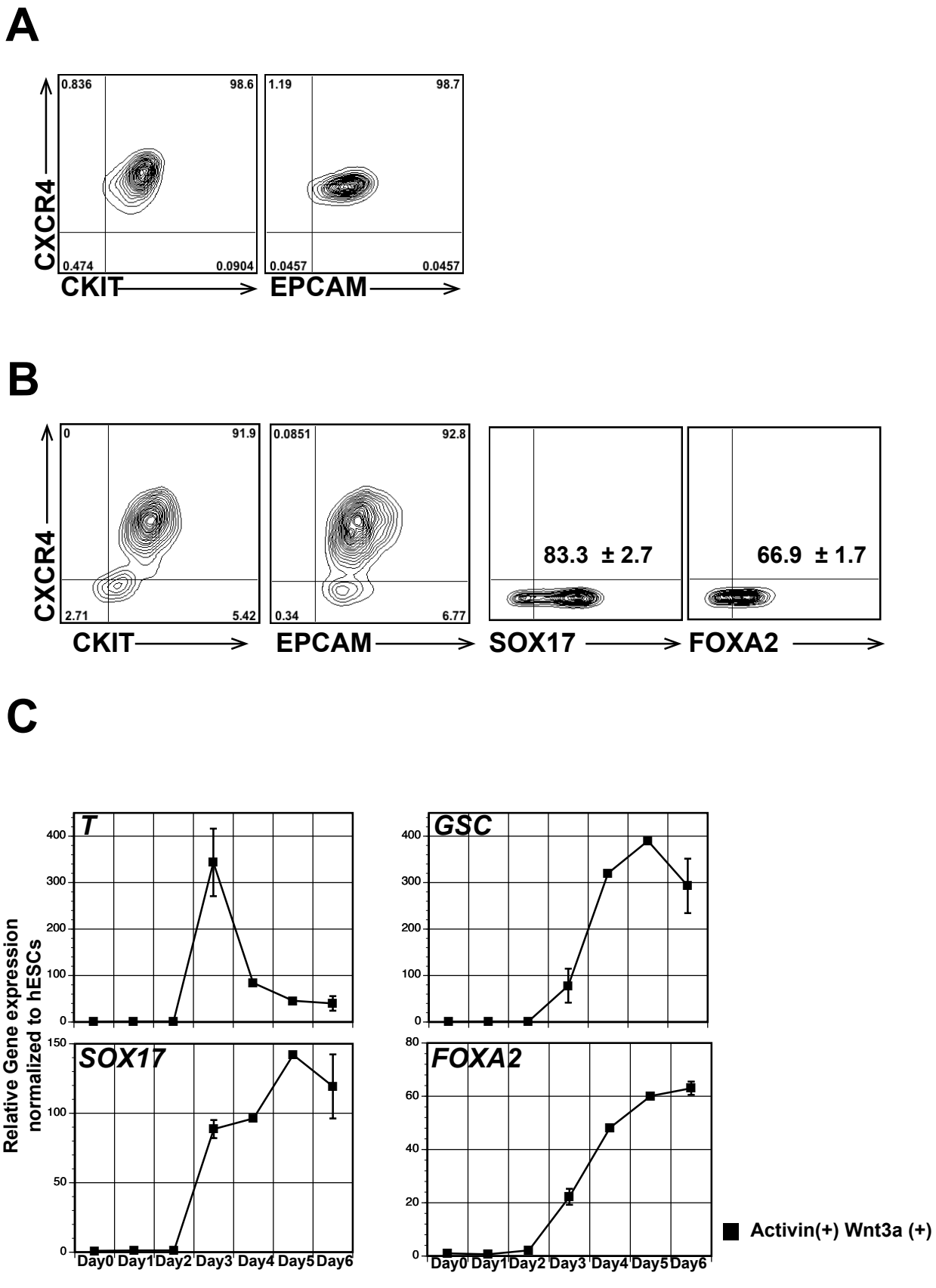

Fig. S1. Endoderm induction in hESC-derived embryoid bodies. (**A**) Flow cytometric analysis showing co-expression EPCAM and CXCR4 on day 6 EBs. (**B**) Flow cytometric analysis showing the proportion of $CXCR4^+$, KIT^+, $EPCAM^+$, $SOX17^+$ and $FOXA2^+$ cells in day 6 EBs induced with activin in neural-based medium. (**C**) RT-qPCR based analyses of *T*, *SOX17*, *GSC* and *FOXA2* expression in activin/Wnt3a-induced EBs. EBs were analyzed at the indicated time points. Bars represent s.d. of the mean of three independent experiments.

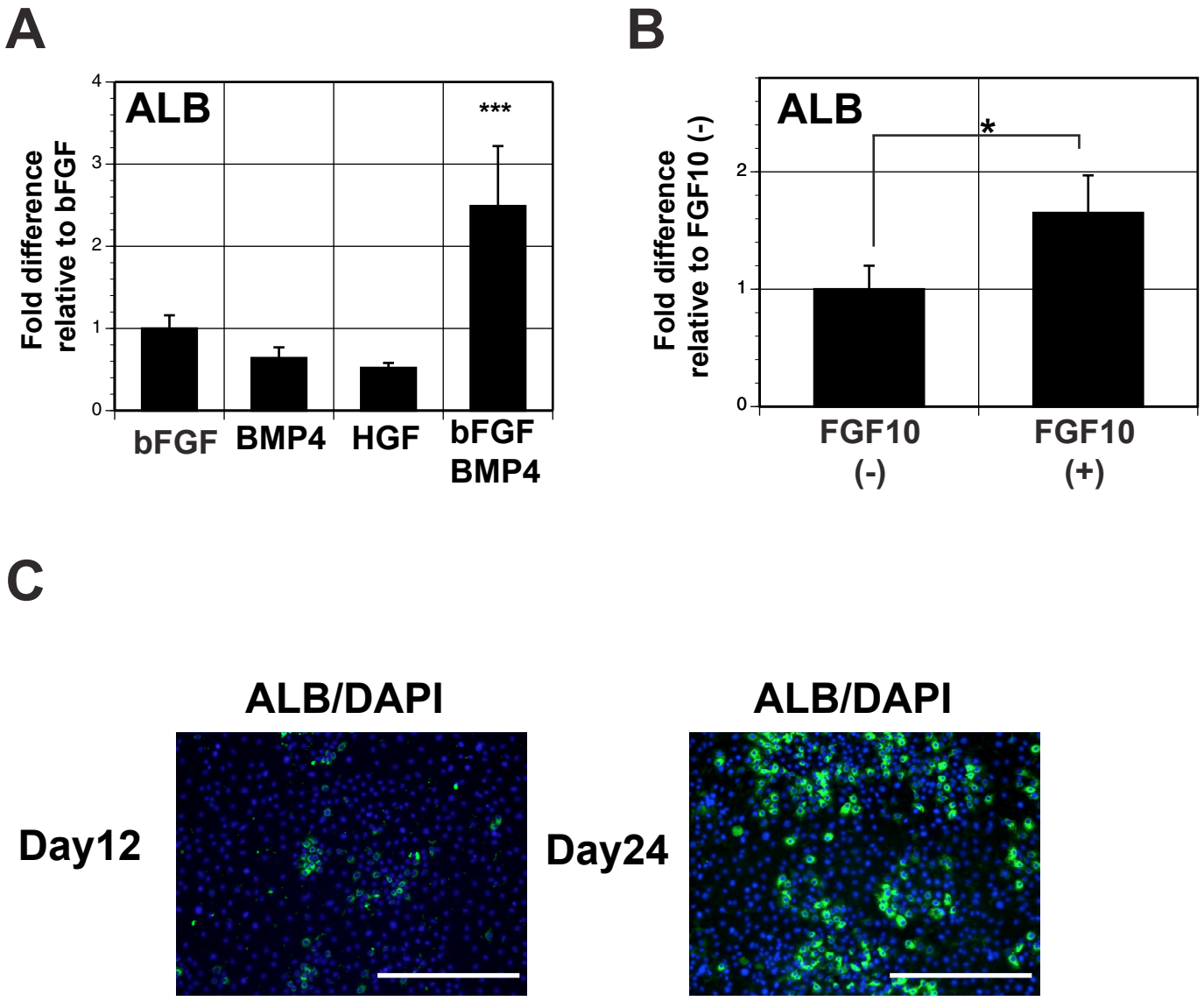

Fig. S2. RT-qPCR analysis of albumin expression in monolayer cultures specified with the indicated cytokines. (**A**) Cells were treated with the different factors (bFGF 10 ng/ml; BMP4 50 ng/ml; HGF 20 ng/ml; or bFGF 20 ng/ml plus BMP4 50 ng/ml) from 6 days to day 12 and then cultured with DEX, HGF and OSM, and analyzed at day 24. Bars represent the s.d. of the mean of three independent experiments. Values are determined relative to *TBP* and presented relative to expression in bFGF (20 ng/ml) culture, which is set to 1. ***P<0.001 when compared with the culture treated with bFGF. Student's t-test, n=3. (**B**) RT-qPCR analysis of albumin expression in populations specified in the presence and absence of FGF10. Cultures were treated (or not) with FGF10 (50 ng/ ml) plus BMP4 (50 ng/ ml) between days 6 and 8. At this stage, the FGF10 was removed and the cells cultured in bFGF/BMP4 between 8 and 12. Bars represent the s.d. of the mean of three independent experiments. Values are determined relative to *TBP* and presented relative to expression in FGF10 (–) culture, which is set to 1. *P<0.05, Student's t-test, n=3. (**C**) Immunostaining analyses showing the presence of ALB+ cells at days 12 and 24 of culture. ALB is visualized with Alexa 488 (green). DAPI (blue) staining shows the nuclei. Scale bar, 200 μm.

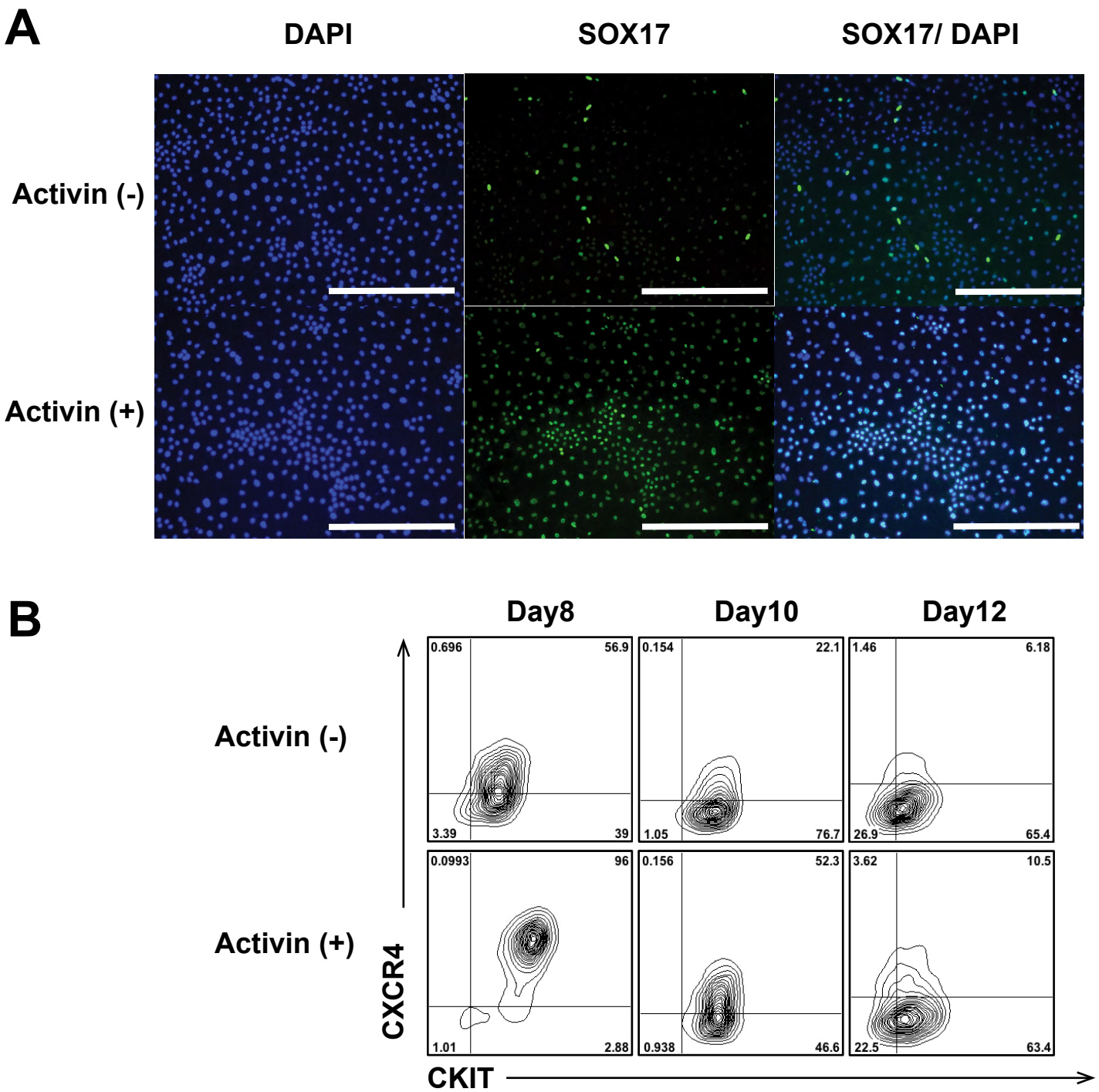

Fig. S3. Duration of nodal/activin signaling impacts hepatic development. (**A**) Immunostaining analyses showing the proportion of SOX17-positive cells in populations generated from non-treated (day 10) and activin-treated (day 12) endoderm. Sox17 is visualized with Alexa 488 (green), nuclei are stained with DAPI (blue). Scale bar: 200 μm. (**B**) Flow cytometric analysis showing the proportion of CXCR4- and KIT-positive cells in populations at days 8, 10 and 12 of culture generated from non-treated cell and activin-treated endoderm

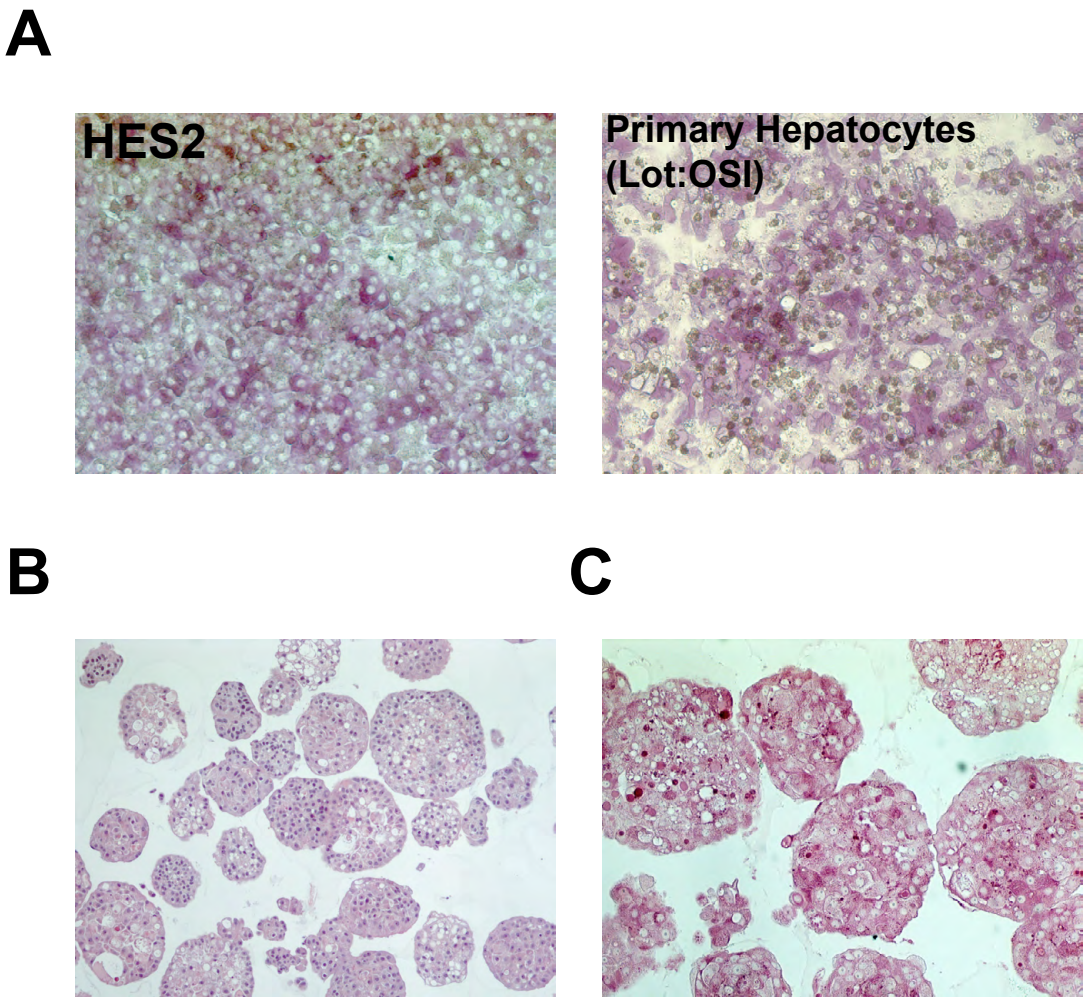

Fig. S4. Periodic acid-Schiff (PAS) staining showing the intracellular storage of glycogen. (**A**) Left: HES2-derived hepatic cells at day 26 of monolayer culture. Right: cryopreserved human hepatocytes (lot OSI) (**B**) Hematoxylin and Eosin staining of HES2-derived aggregates at day 32. (**C**) PAS staining of HES2-derived aggregates at day 32.

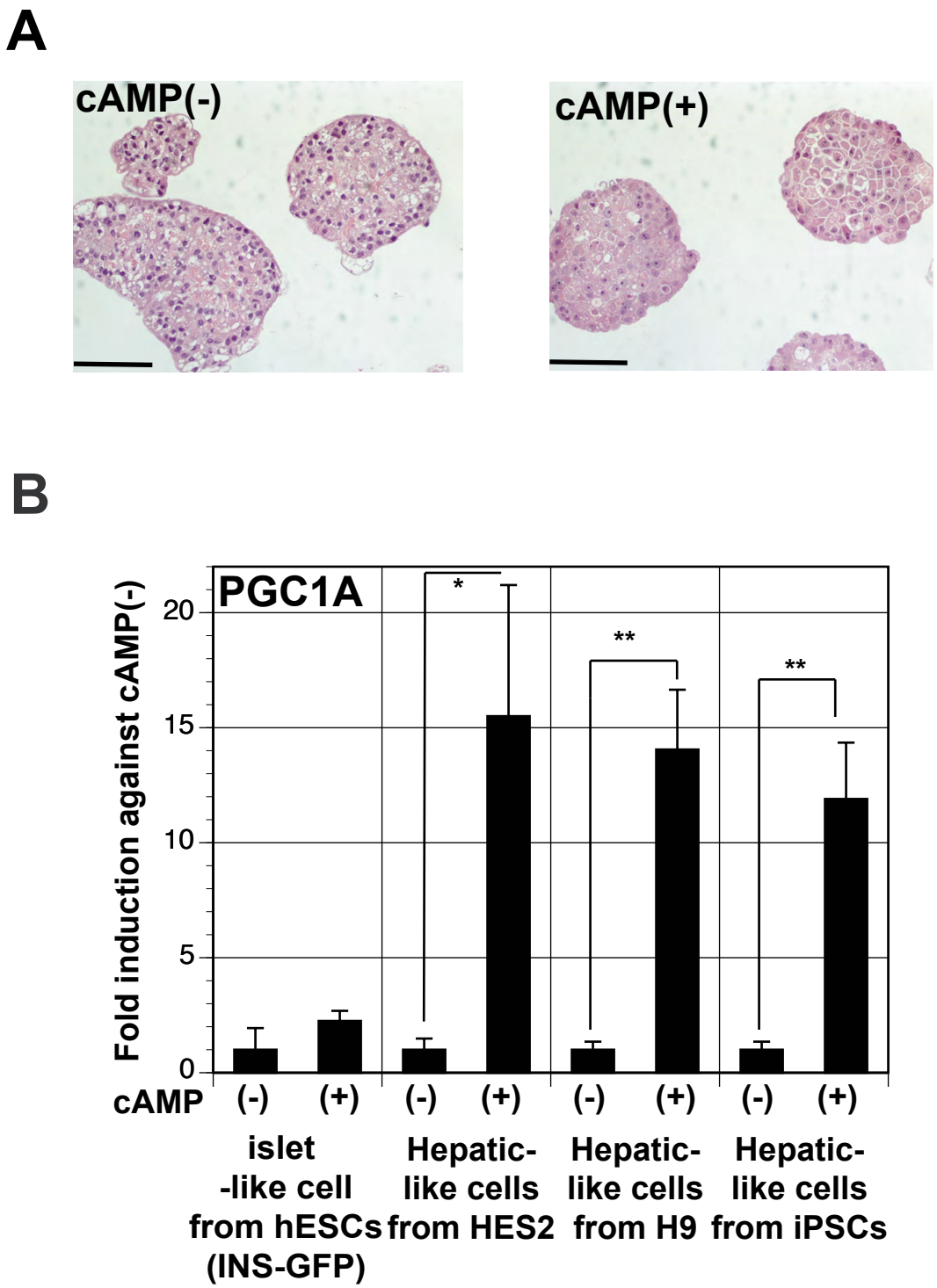

Fig. S5. cAMP signaling induces maturation of hESC-derived hepatocyte-like cells. (**A**) Hematoxylin and eosin staining of 8-Br-cAMP-treated and non-treated HES2-derived aggregates at day 44. (**B**) RT-qPCR analysis of *PGC1*-α expression in cAMP-treated pancreatic aggregates and hepatic aggregates generated from HES2, H9 and 38-2 cells. Values are determined relative to *TBP* and presented as fold change relative to expression in non-treated cells, which is set as 1. Bars represent the s.d. of the mean of three independent experiments, **P*<0.05, ***P*<0.01, ****P*<0.001, Student's *t*-test.

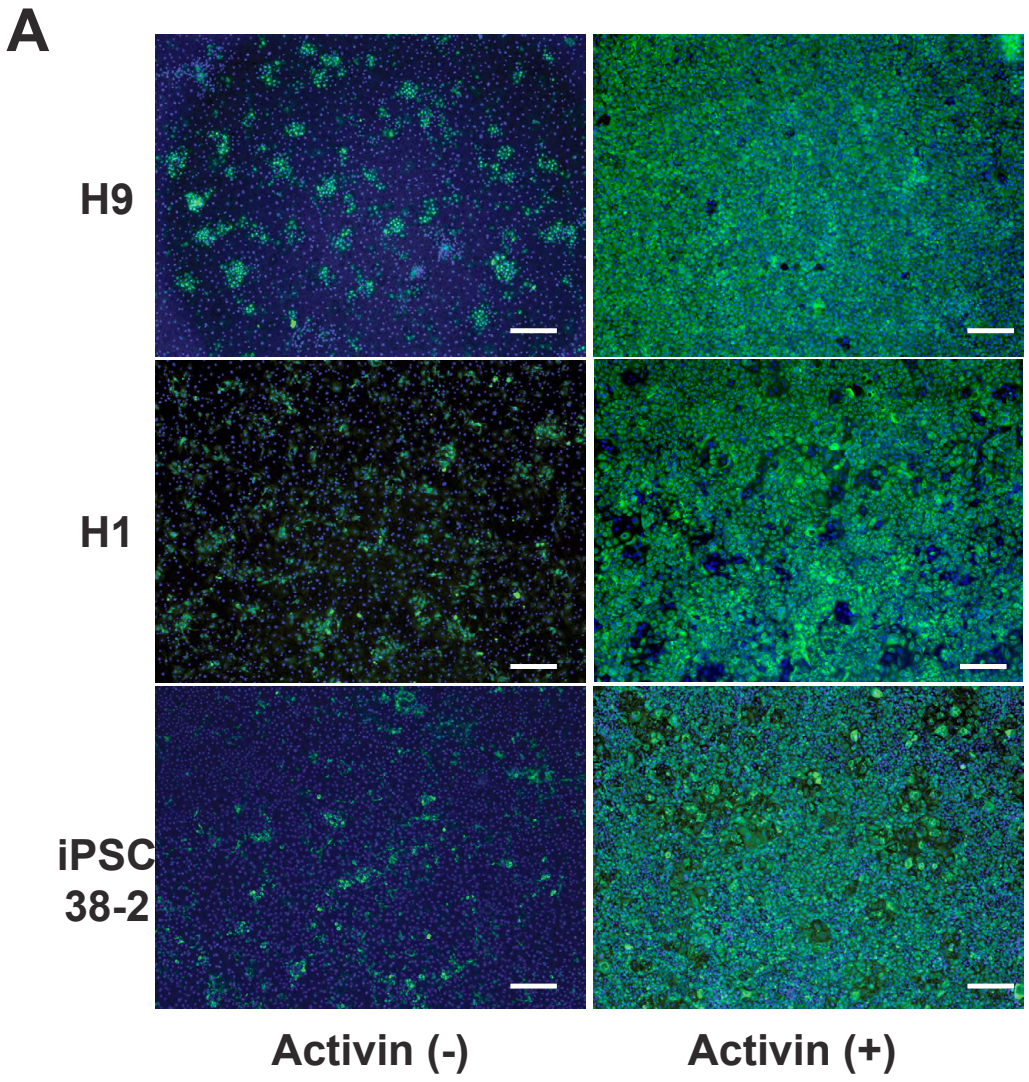

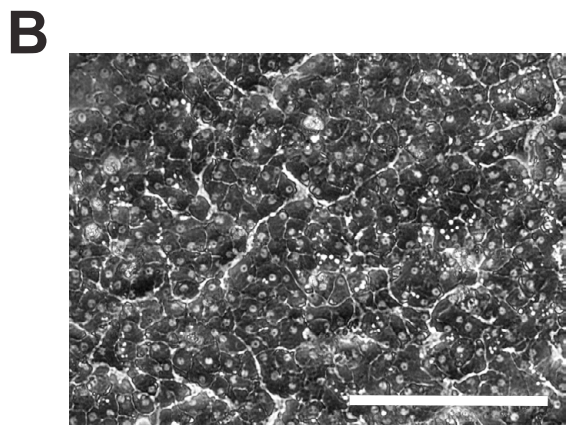

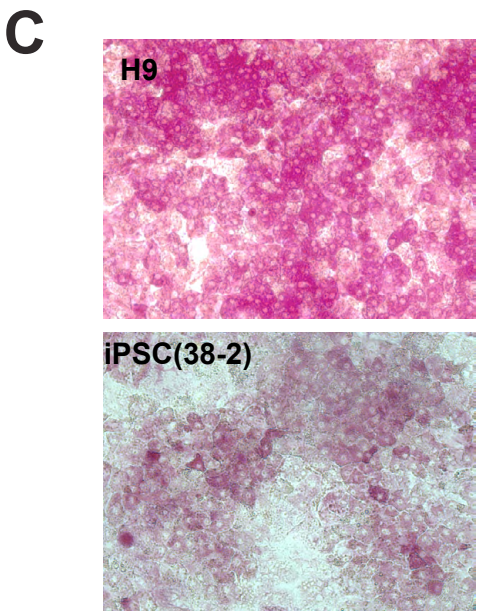

Fig. S6. Hepatic specification and maturation from other hPSC lines. (**A**) Immunostaining analyses showing proportion of ALB-positive cells in cultures generated from activin-treated (day 26-28) and non-treated (day 24) endoderm derived from H9 hESCs, H1 hESCs and 38-2 hiPSCs. ALB is visualized with Alexa 488 (green), nuclei are stained with DAPI (blue). Scale bar: 200 µm. (**B**) Phase-contrast image showing morphology of H9-derived hepatic cells at day 26 of culture. Scale bar: 200 µm. (**C**) PAS staining of H9 hESC- and 38-2 iPSC-derived hepatic cells at day 26.

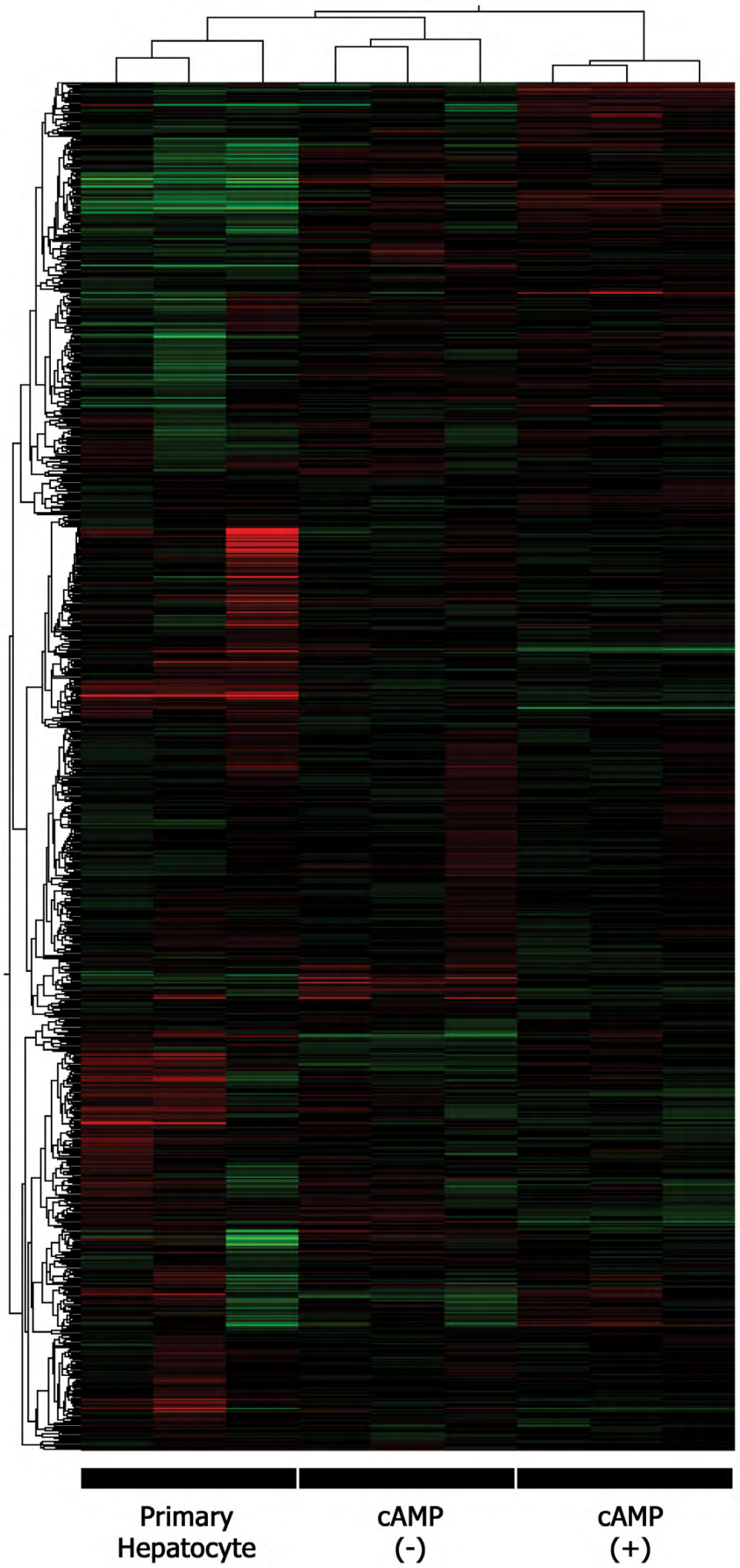

Fig. S7. Heat map summarizing expression of 23038 filtered transcripts, showing the results of a two-way unsupervised hierarchical cluster analysis. Degree of intensity for red and green colors represents the relative amounts of over or underexpression, respectively, compared with median (black) for each transcript.

Table S1. Hepatic specification and maturation from other hPSC cell lines

Hepatic specification and maturation of H9 cells

Culture periods	Based medium	Growth factors and cytokines
Day 8-day 14	H16 DMEM	bFGF (40 ng/ml), BMP4 (50 ng/ml)
Day 14-day 20	H16 DMEM plus 25% Ham's F12 and 0.1% BSA	HGF (20 ng/ml), Dex (40 ng/ml),OSM (20ng/ml)
Day 20-day 32	H21 DMEM plus 25% Ham's F12 and 0.1% BSA	HGF (20 ng/ml), Dex (40 ng/ml),OSM (20 ng/ml)
Day 32-day 44	Hepatocyte culture medium (HCM) (Lonza: CC-4182)	±1 mM 8-bromo-cAMP (Biolab:B007)

Hepatic specification and maturation of H1 and iPS (38-2) cells

Culture periods	Based medium	Growth factors and cytokines
Day 10-day 16	H16 DMEM	bFGF (40 ng/ml), BMP4 (50 ng/ml)
Day 16-day 22	H16 DMEM plus 25% Ham's F12 and 0.1% BSA	HGF (20 ng/ml), Dex (40 ng/ml), OSM (20 ng/ml)
Day 22-day 32	H21 DMEM plus 25% Ham's F12 and 0.1% BSA	HGF (20 ng/ml), Dex (40 ng/ml), OSM (20 ng/ml)
Day 32-day 44	Hepatocyte culture medium (HCM) (Lonza: CC-4182)	±1 mM 8-bromo-cAMP (Biolab:B007)

Table S2. Gene Ontology (GO) analysis

Significantly enriched Gene Ontology (GO) terms upregulated in cAMP(+) lines

GO ID	GO ACCESSION	GO Term	p-value	corrected p-value	Count in Selection	% Count in Selection	Count in Total	% Count in Total
3962	GO:0005737	cytoplasm	6.558086E-5	0.018937081	48	88.888885	7926	44.38844
7176	GO:0009987|GO:0008151|GO:0050875	cellular process	3.710204E-4	0.06418881	24	44.444443	10864	60.842293
20307	GO:0044444	cytoplasmic part	5.3280417E-7	3.769804E-4	23	42.592594	5338	29.894712
3963	GO:0005739	mitochondrion	1.137161E-6	7.151887E-4	20	37.037037	1157	6.4796147
20156	GO:0044237	cellular metabolic process	3.742244E-4	0.06418881	20	37.037037	6802	38.09364
4255	GO:0006082	organic acid metabolic process	2.2573053E-19	8.518051E-16	19	35.185184	621	3.4778225
11694	GO:0019752	carboxylic acid metabolic process	1.6723905E-19	8.518051E-16	19	35.185184	614	3.43862
18201	GO:0042180	cellular ketone metabolic process	3.0354538E-19	8.5908236E-16	19	35.185184	628	3.517025
19372	GO:0043436	oxoacid metabolic process	1.6723905E-19	8.518051E-16	19	35.185184	614	3.43862
20200	GO:0044281	small molecule metabolic process	9.6049245E-12	1.8122323E-8	19	35.185184	2093	11.72155
2603	GO:0003824	catalytic activity	1.0261457E-4	0.02662119	17	31.481482	5422	30.365143
4696	GO:0006629	lipid metabolic process	2.2636464E-9	2.8473262E-6	17	31.481482	879	4.922715
15224	GO:0032787	monocarboxylic acid metabolic process	2.4227023E-15	5.48531E-12	15	27.777779	322	1.8033154
4697	GO:0006631	fatty acid metabolic process	4.5773118E-11	7.402589E-8	11	20.37037	209	1.1704749
20174	GO:0044255	cellular lipid metabolic process	6.67601E-10	9.4470914E-7	11	20.37037	581	3.2538083
26607	GO:0055114	oxidation reduction	1.2482255E-4	0.030065356	11	20.37037	658	3.685036
3997	GO:0005777|GO:0019818	peroxisome	1.3808894E-6	7.8162795E-4	7	12.962963	109	0.61043906
18575	GO:0042579	microbody	1.3808894E-6	7.82E-04	7	12.962963	109	0.61043906
3980	GO:0005759	mitochondrial matrix	2.3700214E-4	0.043983888	6	11.111111	242	1.3552867
4181	GO:0006006	glucose metabolic process	1.5651867E-4	0.031640932	6	11.111111	158	0.88485664
6371	GO:0009056	catabolic process	1.984698E-4	0.03941765	6	11.111111	1919	10.7470875
9242	GO:0016042|GO:0006724	lipid catabolic process	4.8472257E-6	0.00249426	6	11.111111	186	1.0416666
11287	GO:0019318	hexose metabolic process	5.255418E-4	0.08008407	6	11.111111	198	1.108871
14422	GO:0031980	mitochondrial lumen	2.3700214E-4	0.043983888	6	11.111111	242	1.3552867
20292	GO:0044429	mitochondrial part	6.0606044E-6	0.002926196	6	11.111111	661	3.7018368
11362	GO:0019395	fatty acid oxidation	7.766657E-8	6.763351E-5	5	9.259259	43	0.24081542
12838	GO:0030258	lipid modification	1.6807688E-5	0.006795495	5	9.259259	106	0.593638
16857	GO:0034440	lipid oxidation	7.766657E-8	6.763351E-5	5	9.259259	43	0.24081542
20202	GO:0044283	small molecule biosynthetic process	1.8157081E-5	0.006851662	5	9.259259	451	2.5257616
4261	GO:0006090|GO:0006087	pyruvate metabolic process	6.691167E-5	0.018937081	4	7.4074073	43	0.24081542
4262	GO:0006091	generation of precursor metabolites and energy	1.2851076E-5	0.005595479	4	7.4074073	280	1.5681003
4263	GO:0006094	gluconeogenesis	6.203596E-6	0.002926196	4	7.4074073	24	0.13440861
4589	GO:0006519	cellular amino acid and derivative metabolic process	2.7302689E-5	0.009658876	4	7.4074073	308	1.7249104
4590	GO:0006520	cellular amino acid metabolic process	5.5848763E-5	0.017087676	4	7.4074073	261	1.4616935
4700	GO:0006635	fatty acid beta-oxidation	1.7875504E-5	0.006851662	4	7.4074073	31	0.1736111
4911	GO:0006887|GO:0016194|GO:0016195	exocytosis	4.6270303E-4	0.07591444	4	7.4074073	126	0.70564514
6377	GO:0009062	fatty acid catabolic process	1.7585429E-6	9.479923E-4	4	7.4074073	40	0.22401434
6379	GO:0009064	glutamine family amino acid metabolic process	1.0452608E-5	0.004733211	4	7.4074073	57	0.31922042
9254	GO:0016054	organic acid catabolic process	1.565747E-8	1.6113878E-5	4	7.4074073	126	0.70564514
11288	GO:0019319	hexose biosynthetic process	1.5629736E-5	0.006553285	4	7.4074073	30	0.16801076
17052	GO:0034637	cellular carbohydrate biosynthetic process	4.4766616E-4	0.07452749	4	7.4074073	70	0.39202508
20025	GO:0044106	cellular amine metabolic process	4.3171964E-4	0.072945446	4	7.4074073	352	1.9713261
20161	GO:0044242	cellular lipid catabolic process	7.3200616E-5	0.020211663	4	7.4074073	85	0.47603047
20167	GO:0044248	cellular catabolic process	8.693665E-5	0.02343283	4	7.4074073	1682	9.419803
21400	GO:0046165	alcohol biosynthetic process	1.034687E-4	0.02662119	4	7.4074073	48	0.26881722
21566	GO:0046364	monosaccharide biosynthetic process	3.2819313E-5	0.01125866	4	7.4074073	36	0.2016129
21596	GO:0046395	carboxylic acid catabolic process	1.565747E-8	1.6113878E-5	4	7.4074073	126	0.70564514
30	GO:0000038	very long-chain fatty acid metabolic process	2.1062282E-4	0.040413324	3	5.5555553	23	0.12880825
3799	GO:0005496	steroid binding	4.7255788E-4	0.07642371	3	5.5555553	71	0.39762545
4611	GO:0006541	glutamine metabolic process	1.3708798E-4	0.031514384	3	5.5555553	20	0.11200717
4702	GO:0006637	acyl-CoA metabolic process	4.4752804E-5	0.01447516	3	5.5555553	14	0.078405015
4791	GO:0006732|GO:0006752	coenzyme metabolic process	1.2436652E-7	9.386061E-5	3	5.5555553	160	0.89605737
9441	GO:0016289	CoA hydrolase activity	5.5734665E-5	0.017087676	3	5.5555553	15	0.08400538
9443	GO:0016291|GO:0008778|GO:0016292	acyl-CoA thioesterase activity	2.0512542E-5	0.007490813	3	5.5555553	11	0.06160394
15931	GO:0033500	carbohydrate homeostasis	1.5271563E-4	0.031514384	3	5.5555553	53	0.296819
17785	GO:0035383	thioester metabolic process	4.4752804E-5	0.01447516	3	5.5555553	14	0.078405015
18588	GO:0042593	glucose homeostasis	1.5271563E-4	0.031514384	3	5.5555553	53	0.296819
25157	GO:0051186	cofactor metabolic process	1.00181786E-7	8.1008744E-5	3	5.5555553	207	1.1592742
4606	GO:0006536	glutamate metabolic process	1.3708798E-4	0.031514384	2	3.7037036	20	0.11200717
4768	GO:0006706	steroid catabolic process	2.1062282E-4	0.040413324	2	3.7037036	23	0.12880825
9196	GO:0015980	energy derivation by oxidation of organic compounds	6.395557E-7	4.2589311E-4	2	3.7037036	142	0.7952509
9442	GO:0016290|GO:0016293	palmitoyl-CoA hydrolase activity	5.3056213E-4	0.08008407	2	3.7037036	7	0.039202508
15370	GO:0032934|GO:0005498	sterol binding	2.7152587E-4	0.048791237	2	3.7037036	25	0.14000896
15971	GO:0033540	fatty acid beta-oxidation using acyl-CoA oxidase	5.3056213E-4	0.08008407	2	3.7037036	7	0.039202508
16120	GO:0033695	oxidoreductase activity, acting on CH or CH2 groups, quinone or similar compound as acceptor	1.5310886E-4	0.031514384	2	3.7037036	4	0.022401433
17290	GO:0034875	caffeine oxidase activity	1.5310886E-4	0.031514384	2	3.7037036	4	0.022401433
20612	GO:0045333	cellular respiration	1.18166376E-4	0.02908086	2	3.7037036	94	0.5264337

Significantly enriched Gene Ontology (GO) terms up-regulated in the hepatocytes

GO ID	GO ACCESSION	GO Term	p-value	corrected p-value	Count in Selection	% Count in Selection	Count in Total	% Count in Total
1562	GO:0002376	immune system process	3.577121E-12	6.5012102E-9	28	68.29269	1034	5.7907705
4964	GO:0006955	immune response	1.4757004E-12	3.0651428E-9	28	68.29269	670	3.7522402
4080	GO:0005887	integral to plasma membrane	1.14432696E-4	0.08318992	22	53.658535	1257	7.0396504
20282	GO:0044419	interspecies interaction between organisms	7.3517453E-10	1.1876774E-6	17	41.463413	348	1.9489248
25661	GO:0051704|GO:0051706	multi-organism process	1.3370409E-7	1.9439956E-4	17	41.463413	781	4.37388
4961	GO:0006952|GO:0002217|GO:0042829	defense response	1.787167E-6	0.002362235	12	29.268293	644	3.6066308
11793	GO:0019882|GO:0030333	antigen processing and presentation	1.033701E-15	3.7573833E-12	12	29.268293	73	0.40882617
1660	GO:0002474	antigen processing and presentation of peptide antigen via MHC class I	1.875959E-20	2.7275575E-16	11	26.829268	28	0.15681003
18603	GO:0042611	MHC protein complex	2.2178988E-15	6.4494443E-12	11	26.829268	46	0.2576165
18604	GO:0042612	MHC class I protein complex	4.479748E-16	2.1711153E-12	11	26.829268	30	0.16801076
23156	GO:0048002	antigen processing and presentation of peptide antigen	1.6743372E-18	1.2172044E-14	11	26.829268	37	0.20721327
14832	GO:0032393	MHC class I receptor activity	3.54134E-15	8.581574E-12	10	24.390244	25	0.14000896
14345	GO:0031901	early endosome membrane	8.606433E-5	0.07360797	5	12.195122	54	0.30241936
1439	GO:0002253	activation of immune response	2.4822812E-5	0.027762476	4	9.756098	103	0.57683694
1641	GO:0002455	humoral immune response mediated by circulating immunoglobulin	1.2295373E-4	0.085128106	4	9.756098	31	0.1736111
1712	GO:0002526	acute inflammatory response	8.180872E-6	0.009912174	4	9.756098	87	0.4872312
4967	GO:0006958	complement activation, classical pathway	9.402098E-5	0.07594564	4	9.756098	29	0.1624104
24757	GO:0050778	positive regulation of immune response	4.3423148E-5	0.045096606	4	9.756098	153	0.85685486
24045	GO:0050051	leukotriene-B4 20-monooxygenase activity	6.91678E-5	0.06285423	2	4.878049	2	0.011200717

Gene Ontology (GO) analysis showing the gene transcripts in cAMP-induced cells (green) and primary hepatocyte (purple) from Table S9 (Fig. 7A). The cluster showing enhanced expression in the cAMP(+) treated cells is enriched for genes related to liver function. The cluster expressed at the highest level in the primary hepatocytes contains immune system, inflammatory and MHC genes.

Table S3. Phase I drug metabolism enzyme

cAMP(+) versus primary hepatocyte

Gene Symbol	Affymetrix ID	Fold Change cAMP(+) versus hepatocyte	Direction of fold change	Corrected p-value	p-value	Significant in post-hoc Tukey (*P*<0.1)
CYP1A1	7990391	46.071194	up	0.012067234	0.00334378	*
CYP3A7	8141342	21.097319	up	0.017114632	0.0059243	*
CYP2C8|CYP2C19	7935169	16.09552	up	0.012067234	0.00241581	*
CYP2E1	7931643	9.311104	down	0.012067234	0.00289097	*
CYP7A1	8150920	9.042042	up	0.012067234	0.00305444	*
FMO3	7907249	5.937933	down	0.012067234	0.003713	*
CYP1A2	7984862	5.2238216	up	0.012067234	9.765099E-4	*
CYP3A4	8141317	3.6115234	up	0.012067234	0.00104858	*
CYP8B1	8086457	2.8518157	up	0.012067234	0.0037024	*
CYP2C19	7929478	2.6333666	up	0.5220973	0.48193598	
CYP3A5	8141328	2.5988102	up	0.110070765	0.06350236	
CYP2C18	7929466	2.417497	up	0.20925228	0.15291514	
CYP1B1	8051583	2.1679187	up	0.1742982	0.12066799	
FMO5	7919314	2.101705	up	0.121317275	0.07465679	
ADH4	8101852	1.9780805	down	0.01808588	0.00695611	*
CYP7B1	8151056	1.4362873	up	0.08954843	0.04477422	*
CYP2B6	8028963	1.4358941	up	0.071706966	0.03309552	
ADH6	8101862	1.3970135	up	0.095975235	0.05167897	
CYP2C9	7929487	1.3147879	up	0.4188202	0.35438633	
ALDH2	7958784	1.1899356	down	0.06618735	0.02800234	
CYP2D6	8076424	1.1894984	up	0.34041327	0.2749492	
ADH1B	8101881	1.176147	up	0.1742982	0.11466285	
ADH1C	8101893	1.1680543	down	0.6280842	0.6039271	
CYP2A13|CYP2A6|CYP2A7	8028973	1.0301366	down	0.2404887	0.1849913	
ADH1A	8101874	1.0277959	down	0.4814003	0.42585412	
FMO4	7907297	1.0077161	down	0.8514573	0.8514573	

cAMP(+) versus cAMP (–)

Gene Symbol	Affymetrix ID	Fold change cAMP(+) versus	Direction of fold change	p-value	Corrected p-value	Significant in post-hoc Tukey (*P*<0.1)
CYP2C8|CYP2C19	7935169	17.61894	up	0.012067234	0.002415811	*
CYP8B1	8086457	9.690104	up	0.012067234	0.0037024	*
CYP7A1	8150920	8.396973	up	0.012067234	0.003054444	*
CYP3A4	8141317	5.700867	up	0.012067234	0.001048583	*
CYP1A2	7984862	5.6071825	up	0.012067234	9.765099E-4	*
ADH1B	8101881	4.874928	up	0.1742982	0.11466285	
CYP2B6	8028963	4.513215	up	0.071706966	0.033095524	*
CYP1A1	7990391	3.9629219	up	0.012067234	0.003343782	
CYP1B1	8051583	3.9326298	up	0.1742982	0.12066799	
CYP2C9	7929487	2.832749	up	0.4188202	0.35438633	
CYP2C18	7929466	2.1275349	up	0.20925228	0.15291514	
ADH1A	8101874	2.0610342	up	0.4814003	0.42585412	
FMO5	7919314	1.9418982	up	0.121317275	0.074656785	
CYP3A7	8141342	1.670188	up	0.017114632	0.005924296	
CYP3A5	8141328	1.5908221	up	0.110070765	0.063502364	
CYP2D6	8076424	1.4976844	up	0.34041327	0.2749492	
ADH6	8101862	1.4162867	down	0.095975235	0.051678974	
CYP2A13|CYP2A6|CYP2A7	8028973	1.3861729	up	0.2404887	0.1849913	
ADH1C	8101893	1.3693517	up	0.6280842	0.6039271	
CYP2C19	7929478	1.3029042	up	0.5220973	0.48193598	
ALDH2	7958784	1.2843883	up	0.06618735	0.028002342	
CYP7B1	8151056	1.1916578	up	0.08954843	0.044774216	
ADH4	8101852	1.1621644	down	0.01808588	0.006956108	
CYP2E1	7931643	1.1376745	up	0.012067234	0.002890972	
FMO4	7907297	1.1074113	down	0.8514573	0.8514573	
FMO3	7907249	1.027153	up	0.012067234	0.003712995	

A comparison of expression levels of a selected group of Phase I drug metabolism genes between cAMP-treated hepatocyte-like cells and primary hepatocytes (blue) and between cAMP-treated and non-treated hepatocyte-like cells (green).

Table S4. Phase II drug metabolism enzyme

cAMP(+) versus primary hepatocyte

Gene Symbol	Affymetrix ID	Fold Change cAMP(+) VS Hepatocyte	Direction of Fold Change	Corrected p-value	p-value	Significant in Post-hoc Tukey (p<.1)
GSTA2	8127065	8.09758	up	0.045971643	0.0204318	*
SULT2A1	8037949	4.501422	up	0.008581583	0.0012713	*
EPHX1	7910111	4.0226717	up	0.012243672	0.0022673	*
CES1	8001457	3.9624193	down	7.7732874E-4	8.636986E-5	*
EPHX2	8145532	3.5328372	up	0.016735837	0.0050373	*
UGT2B7	8095395	3.345876	up	0.12602992	0.0793522	
GSTA1	8127072	2.7610693	up	0.47513044	0.4223382	
UGT2B7	8100758	2.7340186	up	0.23812853	0.1763915	
UGT2A3	8100760	2.3408983	up	0.12602992	0.0792332	
GSTM2|GSTM4	7903753	2.218478	up	0.016735837	0.0061985	*
UGT3A1	8111512	1.8036636	down	0.10196026	0.0566446	
NAT2	8144866	1.7318547	down	9.925069E-6	.6759516E-	*
SULT1E1	8100808	1.4051794	up	8.63045E-5	.3929256E-	*
SULT1A3|GIYD1|GIYD2|SULT1A2|SULT1A4	7994582	1.4016013	up	0.22789103	0.1603678	
UGT1A1|UGT1A6|UGT1A10|UGT1A9|UGT1A4|UGT1A3|UGT1A5|UGT1A7|UGT1A8	8049349	1.4001894	up	0.016735837	0.0050807	
UGT2B4	8100784	1.3952446	up	0.016735837	0.0055956	
SULT1A2	8000582	1.3303971	down	0.59399104	0.5499917	
UGT2B28	8095404	1.3045363	down	0.07000782	0.0337075	*
GSTA3	8127087	1.2955159	up	0.0954211	0.0494776	*
SULT1A1	8000590	1.2795404	down	0.43535653	0.3708593	
GSTK1	8136849	1.2583706	up	0.03604819	0.0146863	*
CES2	7996345	1.1977214	up	0.016735837	0.0052718	
UGT2B17	8100734	1.1170508	up	0.3367106	0.2743568	
GSTM2	7919578	1.1149695	up	0.22247058	0.1483137	
GSTO1	7930304	1.0659491	up	0.9567845	0.9567845	
UGT2A1|UGT2A2	8100791	1.0262581	up	0.3367106	0.2642122	

cAMP(+) versus cAMP (–)

Gene Symbol	Affymetrix ID	Fold Change cAMP(+) VS cAMP(-)	Direction of Fold Change	p-value	Corrected p-value	Significant in Post-hoc Tukey (p<.1)
UGT1A1|UGT1A6|UGT1A10|UGT1A9|UGT1A4|UGT1A3|UGT1A5|UGT1A7|UGT1A8	8049349	9.1351	up	0.016735837	0.005080654	*
SULT2A1	8037949	4.9485445	up	0.008581583	0.001271346	*
EPHX1	7910111	4.8572507	up	0.012243672	0.002267347	*
CES1	8001457	4.7324886	up	7.7732874E-4	8.636986E-5	*
SULT1E1	8100808	4.077046	down	8.63045E-5	6.3929256E-6	*
GSTA1	8127072	3.6004374	up	0.47513044	0.42233816	
GSTA2	8127065	3.5906198	up	0.045971643	0.02043184	
UGT2B7	8095395	3.5550861	up	0.12602992	0.07935217	
UGT2B4	8100784	3.4201937	up	0.016735837	0.005595609	*
CES2	7996345	3.3923113	up	0.016735837	0.005271834	*
UGT2B7	8100758	2.0410874	up	0.23812853	0.1763915	
EPHX2	8145532	2.0409768	up	0.016735837	0.005037259	*
UGT2A3	8100760	1.3768438	down	0.12602992	0.07923323	
GSTA3	8127087	1.3496046	up	0.0954211	0.049477607	*
SULT1A3|GIYD1|GIYD2|SULT1A2|SULT1A4	7994582	1.2940637	up	0.22789103	0.16036776	
GSTK1	8136849	1.2272205	up	0.03604819	0.0146863	*
SULT1A2	8000582	1.1342998	down	0.59399104	0.5499917	
GSTO1	7930304	1.064542	up	0.9567845	0.9567845	
UGT2A1|UGT2A2	8100791	1.0529388	up	0.3367106	0.2642122	
NAT2	8144866	1.0509218	down	9.925069E-6	3.67595516E-7	
UGT2B28	8095404	1.0417112	down	0.0700078	0.03370747	
NAT1	8144857	1.0342079	down	0.7743908	0.74570966	
UGT2B17	8100734	1.0268425	down	0.3367106	0.27435678	
GSTM2|GSTM4	7903753	1.0195614	down	0.016735837	0.006198458	
SULT1A1	8000590	1.0132033	down	0.43535653	0.37085927	
UGT3A1	8111512	1.0086902	up	0.10196026	0.056644585	
GSTM2	7919578	1.0031872	up	0.22247058	0.14831372	

Transporters

cAMP(+) versus primary hepatocyte

Gene Symbol	Affymetrix ID	Fold Change cAMP(+) VS Hepatocyte	Direction of Fold Change	Corrected p-value	p-value	Significant in post-hoc Tukey (*P*<0.1)
ABCB1	8140782	5.399585	down	0.074096315	0.03554574	*
ABCB4	8140752	4.592113	down	0.01389056	0.00231509	*
ABCB11	8056583	3.9600024	up	0.01389056	0.00126014	*
SLCO1B1	7954356	3.4501076	up	0.036024522	0.00900613	*
SLC10A1	7979878	1.8501159	down	0.39103138	0.3258595	
SLCO2B1	7942569	1.7992761	up	0.47115463	0.43488163	
ABCC3	8008454	1.562891	down	0.074096315	0.03704816	*
ABCC2	7929779	1.5118597	up	0.07192941	0.02397647	
SLC22A10	7940737	1.436169	down	0.47115463	0.47115463	
SLCO1B3	7954344	1.2984133	down	0.12872237	0.07508805	
SLC22A7	8119782	1.2072212	up	0.13624907	0.09083271	
SLCO1A2	7961626	1.082006	up	0.16357224	0.12267918	

cAMP(+) versus cAMP (–)

Gene Symbol	Affymetrix ID	Fold change cAMP(+) VS cAMP(–)	Direction of Fold Change	p-value	Corrected p-value	Significant in post-hoc Tukey (*P*<0.1)
SLCO1B1	7954356	10.375665	up	0.0360245	0.009006131	*
ABCC2	7929779	3.5463655	up	0.0719294	0.023976471	*
ABCB11	8056583	2.6618686	up	0.0138906	0.001260135	*
SLCO2B1	7942569	1.8878269	up	0.4711546	0.43488163	
SLC22A7	8119782	1.8327168	up	0.1362491	0.09083271	
SLC10A1	7979878	1.3948876	up	0.3910314	0.3258595	
ABCB4	8140752	1.1143088	down	0.0138906	0.002315093	
ABCB1	8140782	1.0972914	down	0.0740963	0.035545744	
ABCC3	8008454	1.0846786	up	0.0740963	0.037048157	
SLCO1B3	7954344	1.052959	up	0.1287224	0.07508805	
SLC22A10	7940737	1.0351869	down	0.4711546	0.47115463	
SLCO1A2	7961626	1.015178	up	0.1635722	0.12267918	

A comparison of expression levels of a selected group of Phase II drug metabolism and transporters genes between cAMP-treated hepatocyte-like cells and primary hepatocytes (blue) and between cAMP-treated and non-treated hepatocyte-like cells (green).

Table S5. Expression levels of coagulation factors and apolipoproteins

Coagulation factors

cAMP(+) VS Primary Hepatocyte

Gene Symbol	Affymetrix ID	Fold Change cAMP(+) VS Hepatocyte	Direction of Fold Change	Corrected p-value	p-value	Significant in Post-hoc Tukey (p<.1)
F11	8098671	5.6883545	up	0.004182067	5.576089E-4	*
PLG	8123259	3.113888	up	0.002581835	1.7212232E-4	*
F13A1	8123744	2.233513	down	0.54852325	0.40225038	
F10	7970241	1.7014513	up	0.4975024	0.269627	
FGB	8097910	1.6944155	down	0.015524478	0.003104896	*
F13B	7923073	1.6196274	down	0.4975024	0.24436827	
SERPINC1	7922420	1.5490543	down	0.54852325	0.37034133	
VWF	7960464	1.5394	down	0.4975024	0.29850143	
F12	8116033	1.3436115	up	0.6435278	0.60062593	
PROC	8045018	1.245822	down	0.6435278	0.5670104	
PROS1	8089015	1.1732916	down	0.11162717	0.037209056	
F2	7939706	1.117765	down	0.92382735	0.92382735	
PROS1	8089011	1.095369	up	0.5775279	0.4620223	
F7	7970232	1.0684249	down	0.45363718	0.18145487	
F9	8170215	1.0481349	down	0.10211771	0.02723139	

cAMP(+) VS cAMP (-)

Gene Symbol	Affymetrix ID	Fold Change cAMP(+) VS cAMP(-)	Direction of Fold Change	Corrected p-value	p-value	Significant in Post-hoc Tukey (p<.1)
F9	8170215	3.0743692	up	0.10211771	0.02723139	
F11	8098671	2.358331	up	0.004182067	5.576089E-4	*
FGB	8097910	1.4688783	down	0.015524478	0.003104896	*
F7	7970232	1.4170613	down	0.45363718	0.18145487	
PROS1	8089015	1.2703807	down	0.11162717	0.037209056	
F12	8116033	1.1323404	up	0.6435278	0.60062593	
PROS1	8089011	1.1102681	down	0.5775279	0.4620223	
F13B	7923073	1.1000786	down	0.4975024	0.24436827	
F10	7970241	1.0886061	down	0.4975024	0.269627	
F2	7939706	1.0793462	down	0.92382735	0.92382735	
VWF	7960464	1.0779397	down	0.4975024	0.29850143	
SERPINC1	7922420	1.0443034	up	0.54852325	0.37034133	
F13A1	8123744	1.0372078	up	0.54852325	0.40225038	
PROC	8045018	1.0074449	down	0.6435278	0.5670104	
PLG	8123259	1.0009212	up	0.002581835	1.7212232E-4	

Apolipoproteins

cAMP(+) VS Primary Hepatocyte

Gene Symbol	Affymetrix ID	Fold Change cAMP(+) VS Hepatocyte	Direction of Fold Change	Corrected p-value	p-value	Significant in Post-hoc Tukey (p<.1)
APOA1	8077185	5.7201715	up	0.006371556	0.001820445	*
APOC3	7944035	2.7706282	up	0.08003705	0.045735456	*
APOB	8050619	1.7165838	up	0.006371556	0.001291146	*
APOA2	7921834	1.5493222	up	0.15048462	0.11079896	
APOC2	8029551	1.4680355	up	0.056342013	0.024146577	
APOC1	8029536	1.1765927	up	0.31744564	0.31744564	
APOC4	8029541	1.1487213	down	0.15048462	0.12898682	

cAMP(+) VS cAMP (-)

Gene Symbol	Affymetrix ID	Fold Change cAMP(+) VS cAMP(-)	Direction of Fold Change	Corrected p-value	p-value	Significant in Post-hoc Tukey (p<.1)
APOC2	8029551	2.429501	up	0.056342013	0.024146577	*
APOA1	8077185	1.8780366	up	0.006371556	0.001820445	
APOC1	8029536	1.5829909	up	0.31744564	0.31744564	
APOC3	7944035	1.4547877	up	0.08003705	0.045735456	
APOB	8050619	1.1659406	down	0.006371556	0.001291146	
APOA2	7921834	1.1425041	up	0.15048462	0.11079896	
APOC4	8029541	1.0462136	up	0.15048462	0.12898682	

A comparison of expression levels of a selected group of coagulation factor and apolipoprotein genes between cAMP-treated hepatocyte-like cells and primary hepatocytes (blue) and between cAMP-treated and non-treated hepatocyte-like cells (green).

Table S6. Expression levels of liver related genes, nuclear receptors and transcriptional factors

Liver genes of interest

cAMP(+) VS Primary Hepatocyte

Gene Symbol	Affymetrix ID	Fold Change cAMP(+) VS Hepatocyte	Direction of Fold Change	Corrected p-value	p-value	Significant in Post-hoc Tukey (p<.1)
AFP	8095646	65.93792	up	1.00699835E-4	4.378254E-6	*
AGXT	8049737	4.618539	up	0.013570489	0.006858653	*
AKR1C4	7925939	1.1564364	up	0.028816327	0.021172486	
AKR1D1	8136459	4.816972	up	0.010609764	0.003690352	*
ALB	8095628	2.048784	up	0.047936797	0.039599963	*
ALDOB	8162884	2.979772	up	0.013570489	0.007301067	*
ARG1	8122058	4.721421	up	0.013570489	0.007670276	*
ASGR1	8012043	2.2643049	up	0.011706066	0.005089594	*
ASGR2	8012028	1.2812967	up	0.47513378	0.4544758	
BAAT	8162870	4.6314807	up	0.020830221	0.013584927	*
CPS1	8048026	5.977915	up	0.038876355	0.030424973	*
CPT1A	7949971	6.476342	up	5.8171514E-4	1.01167854E-4	*
CTPS	7900510	1.7996519	up	0.004022882	0.001224356	*
FAH	7985268	2.0180252	up	0.06254039	0.05710209	*
G6PC	8007429	22.897436	up	0.001131729	2.5702044E-4	*
HMGCS2	7919055	34.45101	up	0.001131729	2.9523356E-4	*
HP	7997188	3.59377	down	0.01160576	0.004541385	*
OTC	8166769	3.481216	up	0.058319274	0.050712414	*
PCK1	8063590	30.076572	up	3.0852502E-4	2.6828262E-5	*
PCK2	7973530	1.0236868	up	0.9756709	0.9756709	
POR	8133670	4.5288434	up	5.665288E-4	7.389506E-5	*
TAT	8002556	6.752994	up	0.01819622	0.01107596	*
TDO2	8097991	5.6013775	up	0.028816327	0.021299025	*

cAMP(+) VS cAMP (-)

Gene Symbol	Affymetrix ID	Fold Change cAMP(+) VS cAMP(-)	Direction of Fold Change	Corrected p-value	p-value	Significant in Post-hoc Tukey (p<.1)
PCK1	8063590	33.72393	up	3.0852502E-4	2.6828262E-5	*
TAT	8002556	17.730682	up	0.01819622	0.01107596	*
G6PC	8007429	14.40543	up	0.001131729	2.5702044E-4	*
ARG1	8122058	9.107302	up	0.013570489	0.007670276	*
ALDOB	8162884	5.797745	up	0.013570489	0.007301067	*
CPT1A	7949971	5.121549	up	5.8171514E-4	1.01167854E-4	*
BAAT	8162870	5.0343623	up	0.020830221	0.013584927	*
POR	8133670	4.5395484	up	5.665288E-4	7.389506E-5	*
CPS1	8048026	3.4659047	up	0.038876355	0.030424973	
AGXT	8049737	3.361046	up	0.013570489	0.006858653	*
HMGCS2	7919055	3.0780334	up	0.001131729	2.9523356E-4	*
CTPS	7900510	3.069189	up	0.004022882	0.001224356	*
TDO2	8097991	3.0548642	up	0.028816327	0.021299025	*
OTC	8166769	2.8020606	up	0.058319274	0.050712414	
FAH	7985268	2.1173558	up	0.06254039	0.05710209	*
AKR1C4	7925939	1.9009632	up	0.028816327	0.021172486	*
ASGR1	8012043	1.5339662	up	0.011706066	0.005089594	*
HP	7997188	1.353287	down	0.01160576	0.004541385	
AFP	8095646	1.3416045	down	1.00699835E-4	4.378254E-6	
AKR1D1	8136459	1.2814606	down	0.010609764	0.003690352	
ASGR2	8012028	1.0487944	up	0.47513378	0.4544758	
PCK2	7973530	1.0429556	up	0.9756709	0.9756709	
ALB	8095628	1.0322695	up	0.047936797	0.039599963	

Nuclear Receptors and Transcriptional Factors

cAMP(+) VS Primary Hepatocyte

Gene Symbol	Affymetrix ID	Fold Change cAMP(+) VS Hepatocyte	Direction of Fold Change	Corrected p-value	p-value	Significant in Post-hoc Tukey (p<.1)
PPARGC1A	8099633	8.664994	up	6.924728E-4	6.924728E-5	*
PPARA	8073826	4.299654	up	0.006155438	0.001846631	*
RXRA	8159127	3.0369213	up	0.060834873	0.038636036	*
HNF4A	8062823	2.534574	up	0.006155438	0.001739987	*
NR1I3	7921840	2.3120933	up	0.05959569	0.023838276	*
NR1H4	7957835	1.6012238	up	0.5780357	0.52023214	
HNF4G	8146986	1.5168575	up	0.060834873	0.04258441	
NR1I2	8081925	1.5157825	down	0.117566794	0.09405343	
AHR	8131614	1.4667602	up	0.060834873	0.032607585	
RARA	8007084	1.119617	down	0.6022417	0.6022417	

cAMP(+) VS cAMP (-)

Gene Symbol	Affymetrix ID	Fold Change cAMP(+) VS cAMP(-)	Direction of Fold Change	Corrected p-value	p-value	Significant in Post-hoc Tukey (p<.1)
PPARGC1A	8099633	5.670558	up	6.924728E-4	6.924728E-5	*
RXRA	8159127	2.6896641	up	0.060834873	0.038636036	*
PPARA	8073826	2.247845	up	0.006155438	0.001846631	*
NR1I3	7921840	1.9786081	up	0.05959569	0.023838276	*
HNF4A	8062823	1.7265012	up	0.006155438	0.001739987	*
AHR	8131614	1.4156159	down	0.060834873	0.032607585	
HNF4G	8146986	1.1821347	down	0.060834873	0.04258441	
RARA	8007084	1.0773768	up	0.6022417	0.6022417	
NR1I2	8081925	1.0684412	up	0.117566794	0.09405343	
NR1H4	7957835	1.0335269	down	0.5780357	0.52023214	

A comparison of expression levels of a selected group of liver-related genes, nuclear receptors and transcriptional factors between cAMP-treated hepatocyte-like cells and primary hepatocytes (blue) and between cAMP-treated and non-treated hepatocyte-like cells (green).

Table S7. Antibody lists

Primary Antibody List (related to Figure1-6)

Antibody	Company	Product Codes	Ig Species	Conjugate	Dilution
AFP	DAKO	A0008	Rabbit	none	1:4000(Flow), 1:2000 (Immuno)
ALB	Bethyl	A80-129A	Goat	none	1:200(Flow), 1:400(Immuno)
ALB	DAKO	A0001	Rabbit	none	1:400(Flow), 1:4000(Immuno)
E-cadherin	BD Biosciences	610181	Mouse	none	1:200 (Immuno)
HNF4α	Santa Cruz	sc-6556	Goat	none	1:200(Immuno)
ASGPR1	Santa Cruz	SC13467	Goat	none	1:100(Flow), 1:100(Immuno)
CD117 (c-KIT)	BD Pharmingen	BD 340529	Mouse IgG1	PE	1:50(Flow)
CD117 (c-KIT)	Invitrogen	CD11705	Mouse IgG1	APC	1:100(Flow)
CD184(CXCR4)	BD Pharmingen	BD 555974	Mouse IgG1	PE	1:100(Flow)
CD184(CXCR4)	BD Pharmingen	BD 555976	Mouse IgG1	APC	1:50(Flow)
CD31	BD Pharmingen	BD 555456	Mouse IgG1	PE	1:10 (Flow)
CD326(EPCAM)	eBioscience	12-9326-73	Mouse IgG1	PE	1:20(Flow)
CD90	BioLegend	328110	Mouse IgG1	PE	1:400(Flow)
FOXA2	Abcam	Ab40874	Rabbit	none	1:50 (Flow)
SOX17	R&D	AF1924	Goat	none	1:40(Flow), 1:100(Immuno)

IgG control List

IgG Control	Company	Product Code	Concentration (Stock)
Goat IgG	Sigma	Sigma I5256	1mg/ml
Rabbit IgG	Jackson Immunoresearch	001-000-003	11mg/ml

Secondary Antibody List

Antibody	Company	Product Code	Dilution
IgG goat anti-Mouse cy3	Jackson Immunoresearch	115-166-071	1:300
IgG Donkey anti Rabbit Cy3	Jackson Immunoresearch	711-165-152	1:300
IgG F(ab')2 Donkey anti- Rabbit (PE)	Jackson Immunoresearch	711-116-152	1:300
IgG Donkey anti-Goat Alexa 488	Invitrogen	A11055	1:400
IgG goat anti-Rabbit Alexa 488	Invitrogen	A11008	1:400

Primary antibody list for flow cytometry and immunofluorescence analysis.

IgG control for flow cytometry and immunofluorescence analysis.

Secondary antibody list for flow cytometry and immunofluorescence analysis.

Table S8. Quantitative PCR primer and RNA RNA lists

qPCR primer list (=related to Figs 1-6)

Gene	Sequences (Forward)	Sequences (Reverse)
AFP	5'- ACAGAGGAACAACTTGAGGCTGTC-3'	5'- AGCAAAGCAGACTTCCTGTTCCTG-3'
ALB	5'- GTGAAACACAAGCCCAAGGCAACA-3'	5'- TCAGCCTTGCAGCACTTCTCTACA -3'
BRY (T)	5'- TGTCCCAGGTGGCTTACAGAT GAA -3'	5'- GGTGTGCCAAAGTTGCCAATACAC -3'
CD31	5'- TTCCTGACAGTGTCTTGAGTGGGT-3'	5'- TTTGGCTAGGCGTGGTTCTCATCT-3'
CD90	5'- ATACCAGCAGTTCACCCATTCAGT-3'	5'- AATTGCTGGTGAAGTTGGTTCGGG-3'
CPS1	5'- AATCTCGCAAGGTGGACTCCAAGA-3'	5'- GGTGTCTGCATCTCTATGCTGCTT-3'
CYP1A2	5'- ATGATGCTGTTTGGCATGGGCAAC-3'	5'- GAACTCCAGTTGCTGTAGCAGGAT-3'
CYP2B6	5'- TCTTCCAGTCCATTACCGCCAACA-3'	5'- GCCGAATACAGAGCTGATGAGTGA-3'
CYP3A4	5'- TTGAGTCAAGGGATGGCACCGTAA-3'	5'- TCTCTGGTGTTCTCAGGCACAGAT-3'
CYP3A7	5'- GCACATCATTTGGAGTGAGCATCG-3'	5'- TGAGAGAACGAATGGATCTAATGGA-3'
CYP7A1	5'- TTACAGGACTGCAGAACACCCTCA-3'	5'- GCACTGGTGAACAACATTGGACCT - 3'
FOXA2	5'- GCATTCCCAATCTTGACACGGTGA-3'	5'- GCCCTTGCAGCCAGAATACACATT-3'
G6P	5'- CTGTCAGGCATTGCTGTTGCAGAA-3'	5'- ATGGCGAAGCTGAACAGGAAGAAG-3'
GSC	5'- ACGATGCTACTTTCTTGCACACGC-3'	5'- ACCCTCCCGGCTCTGTACACTATTTA-3'
HEX	5'- TGGATAGCTCTCAATGTTCGCCCT-3'	5'- TATCGCCCTCAATGTCCACTTCCT-3'
HNF4α	5'- TTCTCCAAAGGCTCCCTGTGTTCT-3'	5'- AACGAGTCTGGTTTCTGAGGCTGT-3'
MEOX1	5'- TGAGGACTGATGGCCAAAGAGCAT-3'	5'- ATCCAAACTCACGTTGACCTCCCT-3'
MESP1	5'- AGCCCAAGTGACAAGGGACAACT-3'	5'- AAGGAACCACTTCGAAGGTGCTGA-3'
OCT4	5'- ATGCATTCAAACTGAGGTGCCTGC-3'	5'- CCACCCTTTGTGTTCCCAATTCCT-3'
PGC1α	5'- GACACTGTGGGTAGCCCATCAAA-3'	5'- ACTTACCACGGCATGAAGGCAATG-3'
SOX17	5'- AGGAAATCCTCAGACTCCTGGGTT-3'	5'- CCCAAACTGTTCAAGTGGCAGACA-3'
TAT	5'- ACCCGAATTTCATCCGAGTGGTCA-3'	5'- AGCACAATGGTAGTGCTGCTCACA -3'
TDO	5'- GTGATAGCTCCTACTTCAGCAGTG-3'	5'- ATCAGAGCATCGTGGTGCTGAACA-3'
UGT1A1	5'- GAGAGAGGTGACTGTCCAGGAC-3'	5'- CAAATTCCTGGGATAGTGGATTTT-3'
TBP	5'- TGAGTTGCTCATACCCTGCTGCTA-3'	5'- CCCTCAAACCAACTTGTCAACAGC-3'
TBP (for UGT1A1)	5'- TGTGCACAGGAGCCAAGAGT-3'	5'- ATTTTCTTGCTGCCAGTCTGG-3'

RNA list (related to Figs 1-7)

	RNA	Source	Sex	Lot	Company	Product number
AL1	human adult liver	51-years old	male	7030173	Clontech	636531
AL2	human adult liver	pooled from 30,44 and 55 years old 3 individual	male and female	603161	Agilent Technologies	540017
FL1	human fetal liver	pooled from 63 sponatneously aborted fetus, aged 22-40 weeks	male and female	7030173	Clontech	636540
FL2	human fetal liver	20 weeks fetus	female	601607	BioChain	R1244149-50
PH1	primary cultured hepatocyte	1- year-old	male	HH1892	from Stephen Strom	
PH2	primary cultured hepatocyte	14 months- old	male	HH1901	from Stephen Strom	
PH3	Human hepatocyte	48- years old	male	ZBH2199	Zenbio	RNA-L10-2

Download Table S9

Download Table S10

Download Table S11